

1 **We express our gratitude to Referee #1 for his comments and remarks**

2 the Creative Commons Attribute 3.0 License.

3 **Interactive comment on “Theoretical analysis of mixing in liquid clouds – Part 3:**  
4 **Inhomogeneous mixing” by M. Pinsky et al.**

5  
6 **Anonymous Referee #1**

7 Received and published: 23 January 2016

8 Review of “Theoretical analysis of mixing in liquid clouds”, in three parts. Overall  
9 recommendation: reject and encourage rewriting and resubmission. General comments to all  
10 three parts (repeated in all three reviews). I read the papers with considerable interest mostly  
11 because this seemed to be a popular topic some time ago, in both observations and modeling. I  
12 was curious to see what new these manuscripts bring. Frankly, I was disappointed.

13  
14 © First, the analysis concerns a highly idealized problem, with little applications to real  
15 clouds. Turbulent mixing in clouds is by far more complicated than situations depicted in Fig.  
16 1 of part 1 (and then repeated in different shapes as Figs. 1 in Part 2 and 3). Second, I am  
17 aware of a study in which the authors developed a fairly sophisticated model of microphysical  
18 evolution during turbulent stirring (Jarecka et al., JAS 2013) aiming at prediction of the  
19 homogeneity of mixing. They applied the model to LES simulations of shallow convective  
20 cloud fields. The impact was surprisingly small and the authors of that paper argued why this  
21 might be so (the entrained air comes from the descending shell and is not far from saturation).  
22 So in a sense the subject is “old

23 news”. Finally, the lengthy discussions, full of unnecessary caveats and references to details  
24 of small multi-panel figures, made the reading frustrating. All three parts read like a student  
25 dissertation, not a concise scientific paper highlighting key points and leaving the rest for the  
26 reader to follow. Thus, I read the manuscripts with decreasing interest, and my comments are  
27 more detailed for the part 1, and get more general for parts 2 and 3.

28 Overall, I do not believe that the subject matter deserves close to 100 pages and close to 50  
29 figures. I feel that the material deserves a single, short and concise manuscript, with new  
30 material clearly separated from what I feel has been discussed in the past, perhaps not at such  
31 a level of detail. Reading introductions to all three parts made me mad, because all three say  
32 basically the same thing with different language and organization. Part 1 is mostly trivial in  
33 my view, with some parts speculative and other repeating already published material (see  
34 detailed comments). Parts 2 and 3 have some aspects that perhaps deserve to be published, but  
35 it is not clear to me how useful these are (not very much in my opinion). References to aircraft

36 observations are vague and missing the key aspect, which is the irrelevance of an idealized  
37 problem considered by the authors to low-spatial resolution observations of a complicated  
38 multiscale natural system.

39

40 © General comments to all three parts (repeated in all three reviews). I read the papers with  
41 considerable interest mostly because this seemed to be a popular topic some time ago, in both  
42 observations and modeling. I was curious to see what new these manuscripts bring. Frankly, I  
43 was disappointed. First, the analysis concerns a highly idealized problem, with little  
44 applications to real clouds. Turbulent mixing in clouds is by far more complicated than  
45 situations depicted in Fig. 1 of part 1 (and then repeated in different shapes as Figs. 1 in Part 2  
46 and 3). Second, I am aware of a study in which the authors developed a fairly sophisticated  
47 model of microphysical evolution during turbulent stirring (Jarecka et al., JAS 2013) aiming  
48 at prediction of the homogeneity of mixing. They applied the model to LES simulations of  
49 shallow convective cloud field. The impact was surprisingly small and the authors of that  
50 paper argued why this might be so (the entrained air comes from the descending shell and is  
51 not far from saturation). So in a sense the subject is “old news”. Finally, the lengthy  
52 discussions, full of unnecessary caveats and references to details of small multi-panel figures,  
53 made the reading frustrating. All three parts read like a student dissertation, not a concise  
54 scientific paper highlighting key points and leaving the rest for the reader to follow. Thus, I  
55 read the manuscripts with decreasing interest, and my comments are more detailed for the part  
56 1, and get more general for parts 2 and 3.

57

58 Overall, I do not believe that the subject matter deserves close to 100 pages and close to 50  
59 figures. I feel that the material deserves a single, short and concise manuscript, with new  
60 material clearly separated from what I feel has been discussed in the past, perhaps not at such  
61 a level of detail. Reading introductions to all three parts made me mad, because all three say  
62 basically the same thing with different language and organization. Part 1 is mostly trivial in  
63 my view, with some parts speculative and other repeating already published material (see  
64 detailed comments). Parts 2 and 3 have some aspects that perhaps deserve to be published, but  
65 it is not clear to me how useful these are (not very much in my opinion). References to aircraft  
66 observations are vague and missing the key aspect, which is the irrelevance of an idealized  
67 problem considered by the authors to low-spatial resolution observations of a complicated  
68 multiscale natural system.

69

® The overview sections, which were copied and pasted for all three different reviews, can be summarized by the following claims:

a) The problem of turbulent mixing in clouds “seemed to be a popular topic some time ago”, but now “the subject is old news”.

b) This study addresses a “highly idealized problem” and uses simplified models in order to describe cloud mixing.

c) The results presented in the papers are not new and are “repeating already published material”.

The authors strongly disagree with the above statements of Referee 1.

In response to the first claim: the mechanism of mixing is still not well understood and continues to be a highly relevant problem in the cloud physics community, especially given the high rate of recent publications on this topic. We believe that the three papers contribute significantly to the theory of interaction of cloud droplets with turbulent environment and present novel techniques of investigating the effect of mixing both from a theoretical standpoint and through in-situ observations.

Second, in contrast to the reviewer, we support the common practice of using idealized models of complex cloud processes, in order to investigate physical mechanisms without being bogged down by the multitude of other processes involved. Idealized considerations (e.g. adiabatic assumptions) are widely used in cloud physics as well as in physics in general. The assumptions are clearly articulated at the beginning of each paper in order to let a reader judge about the level of idealization of the utilized approaches.

Third, as regards to novelty, the following new results have been obtained:

a) The first paper suggests a new technique for identifying type of mixing (homogeneous or inhomogeneous) based on the analysis of the moments of droplet size distributions. It was shown that homogeneous mixing breaks functional relationships between the moments. Nothing like that has been done before. A novel approach for identifying mixing from in-situ observations was proposed. The comments obtained by the authors from their colleagues showed that the proposed technique starts to be utilized by other research groups.

b) The second paper considers *homogeneous* mixing. One of the important findings of this paper is an analytical universal solution describing the rate of evolution of microphysical parameters as well as the final equilibrium state (mixing diagram). It is shown that in case of polydisperse droplet size distributions evolution of droplet spectra can lead to an increase in characteristic size of droplets in contrast to the widely accepted “classical” view, when the characteristic droplet size is decreasing. It was shown that evaporation time can be expressed in terms of time of phase relaxation. This is important for the definition of reaction time in the Damköhler number.

c) The third paper is dedicated to *inhomogeneous* mixing. A theoretical framework for a time dependent mixing of two volumes that accompanies by cloud droplet evaporation is developed. A new turbulence-evaporation model of time evolution of ensemble of droplets under different environmental parameters is proposed. In contrast to previous studies the Damkoller number is introduced as a result of re-normalization of mixing-evaporation equation, rather than empirically. It is shown that any mixing leads to droplet spectrum broadening. For the first time the scientifically grounded demarcation between homogeneous and inhomogeneous mixing in the space of environmental parameters is performed.

The authors regret that Referee 1 overlooked all these novelties.

The authors also believe it is impossible to follow the recommendation of Referee 1, to combine all papers into one single, summary paper. While the papers all consider the same subject, they perform completely different functions with regard to investigating the issues of mixing.

70 ©A small technical comment: I think the terminology the papers use is not correct. The  
71 limiting cases should be referred to as homogeneous and extremely inhomogeneous mixing.  
72 Everything between the two is the inhomogeneous mixing.

73

74 ® Strictly speaking, as follows from the analysis in the paper, the limiting case referred to as  
75 extremely inhomogeneous (at which drop radii do not change) corresponds to the absence of  
76 mixing (actually some mixing remains that corresponds to the pure molecular mixing). That is  
77 why we introduced the concept of extremely inhomogeneous mixing as the case when the  
78 mixing process is very slow (very high  $Da$ ). Mixing with smaller  $Da$  is referred to as  
79 inhomogeneous. We also reveal parameters at which homogeneous mixing dominates in some  
80 sense over inhomogeneous. Such cases we refer to as homogeneous mixing.

81

82 Specific comments to Part 3:

83 General comment:

84 © Part 3 discusses an idealized case of the 1D diffusion between initially monodisperse  
85 condensed water volume and subsaturated cloud-free volume. Such a problem is supposed to  
86 mimic the homogenization process in the inhomogeneous mixing scenario. The authors  
87 develop a nondimensional equations and solve them. I really run out of steam to read this part  
88 carefully. Thus, my comments are even less detailed than in the case of Part 2. That said, the  
89 diagram shown in Fig 16 is interesting and with proper exposition may become useful in the  
90 development of subgrid-scale schemes for LES.

91

92 ® We agree that the delimitation introduced between regimes of mixing can be useful for

93 LES. Corresponding discussion about the perspectives of mixing investigation is added into  
94 the conclusion section.

95

96 © How the transitions between various mixing scenarios compare to the outcome of DNS  
97 simulations reported in Andrejczuk et al (2009)? That paper is not even mentioned, but I think  
98 it is relevant, like the Krueger's EMPM model mentioned in the conclusion section.

99

100 ® The approaches are quite different. In our study time evolution of DSD and their moments  
101 as well as other parameters like RH in course on mixing are investigated. Andrejczuk et al  
102 (2009) present only final results of DNS simulations in the form resembling the standard  
103 mixing diagrams.

104 The references to the studies by Andrejczuk et al (2009) and Krueger's (EMPM model) are  
105 included.

106

107 ©And what about the Jensen et al. (JAS, 1985) predictions (not mentioned either)?

108

109 ® The study by Jensen et al. (1985) assumes that cloudy air has two sources: air coming from  
110 cloud base and air coming from cloud top. A method of calculation of cloud parameters in the  
111 case of multiple penetrations of dry volumes into the cloud air is proposed. The approach is  
112 tested using a model of ascending cloud parcel. The approach and subject of investigations in  
113 the study by Jensen et al. (1985) and in the present study are quite different.

114

115 Overall, I find Part 3 the most promising and I feel that focusing on results discussed in Part 3  
116 should be the goal of the new paper.

117

118 ® We also suppose that Pt 3 contains interesting results. As regards to the new paper, see our  
119 response above.

120

121 Specific comments:

122

123 © 1. The time scale describing droplet evaporation is again taken as the phase relaxation time  
124 scale (and used to define the Domkoehler number applied in the investigation). Part 2 shows  
125 (not surprisingly) that this is the correct time scale for the homogeneous mixing. I am not  
126 convinced that the same applies to the inhomogeneous mixing.

127

128 ® In our response to corresponding comment of Reviewer to Part 2 we showed that the phase  
129 relaxation time is a natural characteristic time of the mixing process, because this time  
130 determines both the time evolution of sub-saturation over ensemble of droplets and also time  
131 evolution of liquid water mass.

132 The fact that the drop relaxation time is the natural time scale at any type of mixing is  
133 clearly follows from the non-dimensional form of diffusion-evaporation equation showing  
134 that  $Da$  is the ratio of mixing time to the drop relaxation time.

135 Corresponding comments are included into the text and in the Conclusion section.

136

137 © In the limiting case of the extremely inhomogeneous mixing (which in the current setup  
138 corresponds to the mixing coefficient taken as the molecular diffusivity), the rate of the  
139 homogenization progress depends also on the initial humidity of the cloud-free volume,  
140 doesn't it? Thus, the time-scale of droplet evaporation should be some combination of the  
141 information provided by the phase relaxation time scale and the humidity of the cloud-free  
142 volume.

143

144 ® The reviewer is correct. Yes, it is shown that the mixing -evaporation process depends on  
145 two parameters,  $Da$  and  $R$ . The parameter  $R$  is related to the initial humidity of the cloud-free  
146 volume. These two parameters determine process of mixing at any regime, not only in the  
147 case of the extremely inhomogeneous mixing.

148

149 © Note that the other time scale that can be used (calculated as the time required for the total  
150 evaporation of a single droplet as used in Jarecka et al. I think) excludes droplet  
151 concentration. However, droplet concentration clearly is a relevant parameter in the problem  
152 of the cloud interface propagation due to molecular diffusion in the 1D problem considered by  
153 the authors. Thus, I feel that 1D results applying molecular mixing can be used to calculate  
154 the proper time scale for the homogenization and to explore which time scale (the phase  
155 relaxation or the evaporation) is more appropriate.

156

157 ® As we showed above, the characteristic time scale of the evaporation process is the phase  
158 relaxation time. This time is automatically follows from non-dimensional equations  
159 containing  $Da$ . In our 1-D problem we use averaged equations, so effects of turbulence are  
160 described using coefficient of turbulent diffusion. At the averaging scales there are clear  
161 definitions of concepts of droplet concentration, supersaturation, etc. The scales, where  
162 molecular diffusion dominates (Kolmogorov scales), are of the same order as the distance

163 between two droplets. At these scales the concepts of concentration, supersaturation over the  
164 droplet ensemble become uncertain. We do not consider mixing at such small scales, as it is  
165 mentioned in the paper.

166

167 We deal with turbulent mixing and with turbulent diffusion. The interface between initially  
168 cloud and droplet-free volumes in our problem is of turbulent nature. Corresponding  
169 comments are added into Section 2.

170

171 © 2. Sections 2 and 3 are in my view incomprehensible. Details of the mathematical  
172 derivations should be moved to the appendix and only key formulas should be left in the main  
173 text. Section 4 can be shortened to just a few sentences.

174

175 ® We shortened Section 3. Expressions in Sections 2 should be kept in the main text because  
176 they show the physics of mixing process. Section 4 is very short. The further shortening  
177 would lead to loss of important information about method of solution.

178

179 © 3. I was not able to read through section 5. However, I noticed that the title of section  
180 5.3 is practically the same as section 5.3.2. Shortening (!) and reorganizing is needed.

181

182 ® The title of section 5.3.2 was changed. We do not see the ways to shorten the section 5  
183 without loss of clarity.

184

185 © 4. Can the results be further synthesized? For instance, figures 6 to 9 show time evolutions  
186 of profiles across the simulation domain. Can just one such a figure be shown and outcome of  
187 other simulations be simply presented applying some measure(s) of the evolution? I think this  
188 is what Fig. 16 is showing, but honestly I was too tired reading the three parts to get the points  
189 clearly. Please simplify the discussion and streamline the presentation.

190 ® As was shown in the study, the process of mixing depends on two non-dimensional  
191 parameters:  $Da$  and  $R$ . So, we showed time evolution of most important microphysical  
192 parameters at 3 values of  $Da$  and 3 values of  $R$  (to cover the range of changes of these  
193 parameters). Note that the time evolutions clearly show that times of reaching of final  
194 equilibrium state are quite different, so that in-situ observations hardly show only final states  
195 (as it is generally assumed in analysis of observed data using mixing diagrams).

196 So, we do not see the ways to shorten the Section.

197

198

199 **We express our gratitude to Referee #2 for his valuable comments and remarks.**

200

201 **Comments on “Theoretical investigation of mixing in warm clouds – Part 3:**  
202 **Inhomogeneous mixing”**

203

204 This paper, in my opinion, is the most insightful of the three parts. Analytical results are  
205 obtained for droplet response for an idealized one-dimensional mixing and growth model. The  
206 appearance of the second non-dimensional parameter  $R$ , in addition to the already known  
207 non-dimensional parameter  $Da$ . As illustrated in Figure 16, this opens up a whole new range  
208 of possible conditions for homogeneous versus inhomogeneous mixing. It may help explain  
209 why in some cases observations have seemed to favor one type of mixing limit even when it  
210 was not thought to be dominant. I consider the paper an important theoretical advance in this  
211 now old problem of homogeneous vs inhomogeneous mixing.

212

213 **(R) Thank you.**

214

215 General criticisms:

216 1. As stated already in the reviews of parts 1 and 2, the relationship between this paper and  
217 the previous two papers is weak. Especially this paper is more stand alone. The idealized case  
218 considered here is distinct, and in fact also different compared with the real atmosphere, albeit  
219 still instructive of what may be happening in the fully 3D environment with dynamical  
220 feedbacks, etc. To me, the simplicity is a strength because it allows the underlying physics to  
221 become clearer, but the assumptions and caveats still need to be stated along with those of the  
222 other two parts.

223 **(R) The list of main assumptions and simplifications is included to Section 2.**

224

225 2. The results in this paper are very difficult to interpret in places. For example, there is no  
226 clear physical interpretation of the new dimensionless parameter  $R$ . In fact, it does not even  
227 have a name (in Table 1 it is simply referred to as “non-dimensional parameter). Please come  
228 up with a descriptive name and provide some interpretation. Can you explain what range of  $R$   
229 is realistically achievable in the atmosphere, and how it might vary with typical cloud  
230 conditions?

231

232 **(R) Done. This parameter is now referred to as potential evaporation parameter (PEP).**

233 **Explanations concerning this parameter are presented in Section 3 and in Conclusion.**



234 This parameter formally varies from  $-\infty$ , which corresponds to the cases when either LWC  
 235  $=0$ , to zero when  $RH=100\%$ . When  $R=-1$  means that total evaporation of all droplets leads  
 236 to  $RH=100\%$ . Evaluations show that typical range of  $R$  is between  $-2$  to  $-0.1$ . To evaluate  
 237 the value of  $R$  it is necessary to know LWC and  $RH$  in cloud surrounding.

238

239 3. This is not so much a criticism as a recommendation: can you, based on the findings of  
 240 parts 2 and 3, suggest several specific measurements that could allow the type of mixing in a  
 241 cloud to be identified with less ambiguity than is currently possible? Put another way, how  
 242 can the central findings be experimentally verified? This kind of discussion will be very  
 243 helpful in connecting the theoretical results to the experimental and observational parts of the  
 244 field.

245 (R) Corresponding discussion is added into the conclusion section.

246

247 Specific comments

248

249 1. Figure 1 seems redundant with the previous sections, and is so simple that it can probably  
 250 be deleted and instead described in words.

251

252 (R) fig 1 illustrate the design of the problem.

253

254 2. Check the sign of the second term in Equations 13, 14, 17, 18. It think they should be the  
 255 opposite.

256 (R) Thank you. Corrected.

257 3. Same comment for  $q$  and LWC as in Parts 1 and 2.

258 (R) done

259 4. Same comment for  $S$  as in Part 2.

260 (R) done

261 © 5. Page 30343, line 10: “very” should be “vary”.

262

263 ® The sentence is corrected

264

265 © 6. Page 30347, line 26-28: “at high  $R$ ”, should be “at lower  $R$ ” or “at higher  $|R|$ ”? Also check other  
 266 places in the text. For example: Page 30350, line 18: should be “lower  $|R|$ ”? Page 30351, line 15:  
 267 should be “small  $|R|$ ”?

268

269 ® We checked the values. We added the comment that since  $R < 0$ , larger  $R$  is that closer to  
 270 zero.

271 © 7. Add labels a) and b) in Figure 17.

272 ® done

273

274

275

276

277

278 **Theoretical analysis of mixing in liquid clouds. Part 3: Inhomogeneous mixing**

279

280 M. Pinsky(1), A. Khain(1), and A. Korolev(2)

281

282 (1) Department of Atmospheric Sciences, The Hebrew University of Jerusalem, Israel

283 (2) Environment Canada, Cloud Physics and Severe Weather Section, Toronto, Canada

284

285

286

Submitted to

287

Atmospheric Chemistry and Physics

288

Revised

289

April 2016

290

291

292 Communicating author: Alexander Khain, The Hebrew University of Jerusalem,

293 [khain@vms.huji.ac.il](mailto:khain@vms.huji.ac.il)

294

295

296

297

298

299

300

301

302

303 **Abstract**

304 An idealized diffusion-evaporation model of time-dependent mixing between a cloud  
305 volume and a droplet-free volume is analyzed. The initial droplet size distribution (DSD) in  
306 the cloud volume is assumed to be monodisperse. It is shown that evolution of the  
307 microphysical variables and the final equilibrium state are unambiguously determined by two  
308 non-dimensional parameters. The first one is the potential evaporation parameter  $R$ ,  
309 proportional to the ratio of the saturation deficit to the liquid water content in the cloud  
310 volume, that determines whether the equilibrium state is reached at 100% relative humidity, or  
311 is characterized by a complete evaporation of cloud droplets. The second parameter  $Da$  is the  
312 *Damköhler* number equal to the ratio of the characteristic mixing time to the phase relaxation  
313 time. Parameters  $R$  and  $Da$  determine the type of mixing.

314 The results are analyzed within a wide range of values of  $R$  and  $Da$ . It is shown that there  
315 is no pure homogeneous mixing, since the first mixing stage is always inhomogeneous. The  
316 mixing type can change during the mixing process. Any mixing type leads to formation of a tail  
317 of small droplets in DSD and, therefore, to DSD broadening that depends on  $Da$ . At large  $Da$ ,  
318 the final DSD dispersion can be as large as 0.2. The total duration of mixing varies from  
319 several to one hundred phase relaxation time periods, depending on  $R$  and  $Da$ .

320 The definitions of homogeneous and inhomogeneous types of mixing are reconsidered and  
321 clarified, enabling a more precise delimitation between them. The paper also compares the  
322 results obtained with those based on the classic mixing concepts.

323 **Keywords:** homogeneous and inhomogeneous mixing, turbulent diffusion, droplet  
324 evaporation

325

## 1. Introduction

Cloud physics typically investigates two types of turbulent mixing: homogeneous and extremely inhomogeneous (e.g. Burner and Brenguier, 2006; Andrejczuk et al., 2009; Devenish et al., 2012; Kumar et al., 2012). The concept of extremely inhomogeneous mixing in clouds was introduced by Latham and Reed (1977); Baker and Latham (1979), Baker et al. (1980) and Blyth et al. (1980). According to this concept, mixing of cloud air and sub-saturated air from cloud surrounding results in complete evaporation of a fraction of cloud droplets, whereas size of other droplets remain unchanged. The studies of extremely inhomogeneous mixing were closely related to investigation of different mechanisms underlying enhanced growth of cloud droplets and warm precipitation formation (Baker et al., 1980; Baker and Latham, 1982). The concept of homogeneous mixing suggests that all the droplets partially evaporate, so the liquid water content decreases while the droplet concentration remains unchanged (Lehmann et al., 2009; Pt1). The significance of the concepts of homogeneous and inhomogeneous mixing goes far beyond formation of large-sized droplets. In fact, these concepts are closely related to the mechanisms involved in formation of droplet size distributions (DSD) in clouds and to the description of this formation in numerical cloud models. A detailed analysis of the classical concepts of homogeneous and extremely inhomogeneous mixing is given by Korolev et al. (2016, hereafter Pt1).

Mixing in clouds includes two processes: mechanical mixing caused by turbulent diffusion and droplet evaporation accompanied by increasing relative humidity. The relative contribution of these processes can be evaluated by comparison of two characteristic time scales: the characteristic mixing time scale  $\tau_{mix} \sim L^{2/3} \varepsilon^{-1/3}$  (where  $L$  is the characteristic linear scale of an entrained volume and  $\varepsilon$  is the dissipation rate of turbulent kinetic energy) and the time of phase relaxation  $\tau_{pr} = (4\pi \mathcal{D} \bar{r} N)^{-1}$  (where  $N$  is droplet concentration in a cloud volume,  $\bar{r}$  is the mean droplet radius and  $\mathcal{D}$  is the diffusivity of water vapor) characterizing the response of the droplet population to changes in humidity (the list of notations is given in Appendix). The

352 choice of the phase relaxation time as the characteristic time scale of mixing is discussed by  
353 Pinsky et al. (2016) (hereafter referred to as Pt. 2) and will be further elaborated below.

354 Mixing is considered homogeneous if  $\tau_{mix} / \tau_{pr} \ll 1$ . At the first stage of mixing, the initial  
355 gradients of the microphysical and thermodynamic variables rapidly decrease to zero. By the  
356 end of this stage, the fields of temperature, humidity (hence, the relative humidity, RH) and  
357 droplet concentration are spatially homogenized and all the droplets within the mixing volume  
358 experience the same saturation deficit. During the relatively lengthy second stage, droplets  
359 evaporate and increase the relative humidity in the volume. It was shown that homogeneous  
360 mixing takes place at scales below about 0.5 m (Pt. 2)

361 At spatial scales larger than  $\sim 0.5$  m,  $\tau_{mix} / \tau_{pr} > 1$  and the spatial gradients of RH remain for  
362 a long time. Consequently, droplets within the mixing volume experience different  
363 subsaturations, thus the mixing is considered inhomogeneous. At  $\tau_{mix} / \tau_{pr} \gg 1$ , the mixing is  
364 considered extremely inhomogeneous.

365 According to the classical conceptual scheme, during the first stage of extremely  
366 inhomogeneous mixing a fraction of droplets is transported into the droplet-free entrained  
367 volume and evaporates completely. The evaporation continues until the evaporating droplets  
368 saturate the initially droplet-free volume. At the second stage, turbulent mixing between the  
369 cloud volume and the initially droplet-free (but already saturated) volume homogenizes the  
370 gradients of droplet concentration and other quantities. Since both volumes are saturated,  
371 mixing does not affect droplet sizes. As a result, the final (equilibrium) state is characterized by  
372 the relative humidity  $RH=100\%$  and the DSD shape similar to that before mixing, but with a  
373 lower droplet concentration. The same result (a decrease in droplet concentration but  
374 unchanged droplet size) is expected in cases of both monodisperse and polydisperse initial  
375 DSD. Since the DSD shape does not change, the characteristic droplet sizes (i.e. the mean

376 square radius, the mean volume radius and the effective radius) do not change either in the  
377 course of extremely inhomogeneous mixing.

378 Thus, according to the classical concepts, the final equilibrium state with RH=100% is  
379 reached either by a partial evaporation of all droplets (homogeneous mixing) or a total  
380 evaporation of a certain portion of droplets that does not affect the remaining droplets  
381 (extremely inhomogeneous mixing) (Lehmann et al., 2009; Pt1).

382 In analyses of in-situ measurements, the observed data are usually compared with those  
383 expected at the final state of mixing as assumed by the classical mixing concepts. If droplet  
384 concentration decreases without a corresponding change in the characteristic droplet radius,  
385 the mixing is considered “extremely inhomogeneous.” If the characteristic droplet radius  
386 decreases with an increase of the dilution level while droplet concentration decreases  
387 insignificantly, the mixing is identified as “homogeneous.” If both the characteristic droplet  
388 radius and the droplet concentration change, the mixing is considered as "intermediate".  
389 Quantitative evaluations of the microphysical processes specific for intermediate mixing  
390 remain largely uncertain.

391 As was discussed in Pt 2, the final states of mixing suggested by the classical concepts are  
392 only hypothetical. To understand the essence of the final equilibrium states of mixing and  
393 evaluate the time needed to reach them, it is necessary to consider the time evolution of DSD in  
394 the course of mixing process. Time-dependent process of homogeneous mixing was analyzed  
395 in Pt. 2. It was shown that in important cases of wide polydisperse initial DSDs, the final state  
396 substantially differs from that hypothesized by the classical concepts.

397 In this study, which is a Pt 3 of the set of studies, we analyze the time-dependent process of  
398 inhomogeneous mixing. The structure of the paper is as follows. The main concept and the  
399 basic equations for time-dependent inhomogeneous mixing are described in Section 2. Analysis  
400 of non-dimensional diffusion-evaporation equations is presented in Section 3. The design and  
401 the results of simulations of non-homogeneous mixing are outlined in Sections 4 and 5. A

402 discussion clarifying the concepts of homogeneous and inhomogeneous mixing is presented in  
403 concluding Section 6.

404

## 405 **2. The main concept and the basic equations**

406 During mixing of cloud volume and entrained air volume, the following two processes  
407 determine the change of the microphysical and thermodynamical variables: turbulent diffusion  
408 resulting in mechanical smoothening of the gradients of temperature, water vapor and droplet  
409 concentration, and droplet evaporation accompanied by phase transformation. In this study,  
410 inhomogeneous mixing is investigated based on the analysis and solution of a 1D diffusion-  
411 evaporation equation. To our knowledge, the idea of using a diffusive model of turbulent  
412 mixing to describe the mixing process was first proposed by Baker and Latham (1982). A  
413 diffusion-evaporation equation was also analyzed by Jeffery and Reisner (2006). In order to get  
414 a more precise understanding of the physics of mixing process the analysis is performed under  
415 the following main simplifying assumptions:

416 a) turbulent mixing is analyzed neglecting vertical motions of mixing volumes, droplet  
417 collisions and droplet sedimentation.

418 b) the total mixing volume is assumed adiabatic.

419 c) mixing is assumed to take place only along the  $x$ -direction, i.e. a 1D task is considered;

420 d) the initial DSD in the cloud volume is assumed monodisperse.

421 Other assumptions and simplifications are discussed below.

422

423 A schematic illustration of the initial conditions used in the study is shown in **Figure 1**.  
424 Two air volumes are assumed to mix: a cloud volume (left) and a droplet-free volume (right),  
425 each having the linear size of  $L/2$ . The value of  $L$  is assumed within the range of several tens  
426 to a few hundred meters. The mixing starts at  $t=0$ . The cloud volume is initially saturated  
427  $S_1=0$ , the initial droplet concentration is  $N_1$  and the initial liquid water mixing ratio is

428  $q_1 = \frac{4\pi\rho_w}{3\rho_a} N_1 r_0^3$ . In the droplet-free volume the initial conditions are  $RH_2 < 100\%$  (i.e.  
 429  $S_2 < 0$ ),  $N_2 = 0$  and  $q_2 = 0$ . Therefore, the initial profiles of these quantities along the  $x$ -axis  
 430 are step functions

$$431 \quad N(x,0) = \begin{cases} N_1 & \text{if } 0 \leq x < L/2 \\ 0 & \text{if } L/2 \leq x < L \end{cases} \quad (1a)$$

$$432 \quad S(x,0) = \begin{cases} 0 & \text{if } 0 \leq x < L/2 \\ S_2 & \text{if } L/2 \leq x < L \end{cases} \quad (1b)$$

$$433 \quad q(x,0) = \begin{cases} q_1 & \text{if } 0 \leq x < L/2 \\ 0 & \text{if } L/2 \leq x < L \end{cases} \quad (1c)$$

434 The initial profile of droplet concentration is shown in Fig. 1. In this study, averaged equations  
 435 are used. We do not consider mixing at scales below several millimeters. At the scales of  
 436 averaging, there exist clear definitions of droplet concentration, supersaturation and other "macro  
 437 scale" quantities. The mixing is assumed to be driven by isotropic turbulence within the inertial  
 438 sub-range where the Richardson's law is valid. Accordingly, turbulent diffusion (turbulent  
 439 mixing) is described by a 1D equation of turbulent diffusion with a turbulent coefficient  $K$ . The  
 440 turbulent coefficient is evaluated as proposed by Monin and Yaglom (1975)

441

$$442 \quad K(L) = C\varepsilon^{1/3}L^{4/3} \quad (2)$$

443 In Eq. (2),  $C$  is a constant. Eq. (2) is valid in case turbulent diffusion is considered, i.e. at scales  
 444 where molecular diffusion can be neglected.

445 Since the total mixing volume is adiabatic, the fluxes of different quantities through the left  
 446 and right boundaries of the volume are equal to zero at any time instance, i.e.

$$447 \quad \frac{\partial N(0,t)}{\partial x} = \frac{\partial N(L,t)}{\partial x} = 0; \quad \frac{\partial q(0,t)}{\partial x} = \frac{\partial q(L,t)}{\partial x} = 0; \quad \frac{\partial q_v(0,t)}{\partial x} = \frac{\partial q_v(L,t)}{\partial x} = 0 \quad (3)$$

448 where  $q_v$  is the water vapor mixing ratio.

449 During mixing, droplets in the mixing volume experience different subsaturations,  
 450 therefore, the initially monodisperse DSD will become polydisperse. The droplets that were



451 transported into the initially droplet-free volume will undergo either partial or complete  
 452 evaporation. The evaporation leads to a decrease in both droplet size and droplet concentration.

453 The basic system of equations that describes the processes of diffusion and of evaporation  
 454 which occur simultaneously is to be derived. The first equation is written for value  $\Gamma$  defined  
 455 as

$$456 \quad \Gamma = S + A_2 q \quad (4)$$

457 This value is conservative in a moist adiabatic process, i.e. it does not change during phase  
 458 transitions (Pinsky et al., 2013, 2014). In Eq. (4), the coefficient  $A_2 = \frac{1}{q_v} + \frac{L_w^2}{c_p R_v T^2}$  is a weak

459 function of temperature that changes by  $\sim 10\%$  when temperatures change by  $\sim 10^\circ\text{C}$  (Pinsky et  
 460 al., 2013). In this study, it is assumed that  $A_2 = \text{constant}$ . In Eq. (4),  $q = \frac{4\pi\rho_w}{3\rho_a} \int_0^\infty r^3 f(r) dr$  is the

461 liquid water mixing ratio and  $f(r)$  is the DSD. The quantity  $\Gamma$  obeys the diffusion equation

$$462 \quad \frac{\partial\Gamma(x,t)}{\partial t} = K \frac{\partial^2\Gamma(x,t)}{\partial x^2} \quad (5)$$

463 with the boundary conditions  $\frac{\partial\Gamma(0,t)}{\partial x} = \frac{\partial\Gamma(L,t)}{\partial x} = 0$  and the initial profile at  $t = 0$

$$464 \quad \Gamma(x,0) = \begin{cases} A_2 q_1 & \text{if } 0 \leq x < L/2 \\ S_2 & \text{if } L/2 \leq x < L \end{cases} \quad (6)$$

465 Therefore, function  $\Gamma(x,0)$  is positive in the left volume, and negative in the right volume.

466 Since  $\Gamma$  does not depend on phase transitions, Eq. (5) can be solved independently of other  
 467 equations. The solution of Eq. (5) with initial conditions (6) is (Polyanin and Zaitsev, 2004)

$$468 \quad \Gamma(x,t) = \sum_{n=0}^{\infty} a_n \exp\left(-\frac{Kn^2\pi^2 t}{L^2}\right) \cos\left(\frac{n\pi x}{L}\right) = \quad (7)$$

$$\frac{1}{2}(S_2 + A_2 q_1) + (A_2 q_1 - S_2) \sum_{n=1}^{\infty} \frac{\sin(n\pi/2)}{n\pi/2} \exp\left(-\frac{Kn^2\pi^2 t}{L^2}\right) \cos\left(\frac{n\pi x}{L}\right)$$

469 where the Fourier coefficients of expanding the step function (6) are

$$470 \quad a_0 = \frac{1}{2}(A_2 q_1 + S_2) \quad (8a)$$

$$471 \quad a_n = (A_2 q_1 - S_2) \frac{\sin(n\pi/2)}{n\pi/2}, \quad n = 1, 2, \dots \quad (8b)$$

472 An example of spatial dependencies of  $\Gamma(x, t)$  at different time instances during the mixing is  
 473 shown in **Figure 2**. One can see a decrease in the initial gradients and a tendency to  
 474 establishing a horizontally uniform value of  $\Gamma$ . Since the initial volume was divided into two  
 475 equal parts, the diffusion leads to formation of a constant limit value of function  $\Gamma$

$$476 \quad \Gamma(x, \infty) = \frac{1}{2}(\Gamma(0, 0) + \Gamma(L, 0)).$$

477 The second basic equation is the equation for diffusional droplet growth, taken in the  
 478 following form (Pruppacher and Klett, 2007)

$$479 \quad \frac{d\sigma}{dt} = \frac{2S}{F} \quad (9)$$

480 where  $\sigma = r^2$  is the square of droplet radius and  $F = \frac{\rho_w L_w^2}{k_a R_v T^2} + \frac{\rho_w R_v T}{e_s(T) \mathcal{D}}$ . The value of

481 coefficient  $F$  is considered constant in this study. The solution of Eq. (9) is

$$482 \quad \sigma(t) = \frac{2}{F} \int_0^t S(t') dt' + \sigma_0 \quad (10)$$

483 The third main equation describes the evolution of DSD. In the following discussion, the  
 484 DSD will be presented in the form  $g(\sigma)$  which is the distribution of the square of the radius.  
 485 This formulation directly utilizes the property of the diffusion growth equation (9) according to  
 486 which the time changes of DSD are reduced to shifting the distributions in the space of square  
 487 radii, while the shape of the distribution remains unchanged. The standard DSD  $f(r)$  is related  
 488 to  $g(\sigma)$  as  $f(r) = 2r \cdot g(r^2)$ .

489 The normalized condition for  $g(\sigma)$  is

$$490 \quad N = \int_0^{\infty} g(\sigma) d\sigma \quad (11)$$

491 where  $N$  is the droplet concentration. Using DSD  $g(\sigma)$ , the liquid water mixing ratio can be  
 492 presented as integral

$$493 \quad q = \frac{4\pi\rho_w}{3\rho_a} \int_0^{\infty} \sigma^{3/2} g(\sigma) d\sigma \quad (12)$$

494 The 1D diffusion-evaporation equation for the non-conservative function  $g(\sigma)$  can be  
 495 written in the form (Rogers and Yau, 1989)

$$496 \quad \frac{\partial g(\sigma)}{\partial t} = K \frac{\partial^2 g(\sigma)}{\partial x^2} - \frac{\partial}{\partial \sigma} \left( \frac{d\sigma}{dt} g(\sigma) \right) \quad (13)$$

497 where the first term on the right-hand side of Eq. (13) describes changes in the DSD due to  
 498 spatial diffusion, while the second term on the right-hand side describes changes in the DSD  
 499 due to evaporation. Substitution of Eq. (9) into Eq. (13) leads to the following equation

$$500 \quad \frac{\partial g(x,t,\sigma)}{\partial t} = K \frac{\partial^2 g(x,t,\sigma)}{\partial x^2} - \frac{2S(x,t)}{F} \frac{\partial g(x,t,\sigma)}{\partial \sigma} \quad (14)$$

501 To close Eq. (14), Eq. (4) should be used in the form

$$502 \quad S(x,t) = \Gamma(x,t) - A_2 q(x,t) \quad (15)$$

503 where  $q(x,t)$  is calculated according to Eq. (12). Eqs. (12, 14, 15) constitute a closed set of  
 504 equations allowing calculation of  $g(x,t,\sigma)$ .

505 To proceed to the equations for DSD moments, let us define a moment of DSD  $g(\sigma)$  of  
 506 order  $\alpha$  as

$$507 \quad m_\alpha = \overline{\sigma^\alpha} = \int_0^{\infty} \sigma^\alpha g(\sigma) d\sigma \quad (16)$$

508 Multiplying Eq. (14) by  $\sigma^\alpha$ , integrating within limits  $[0..\infty]$  and assuming that  $\sigma^\alpha g(\sigma) \rightarrow 0$   
 509 when  $\sigma \rightarrow \infty$ , yield a recurrent formula for the DSD moments

510

$$511 \quad \frac{\partial m_\alpha(x,t)}{\partial t} = K \frac{\partial^2 m_\alpha(x,t)}{\partial x^2} + \alpha \frac{2S}{F} m_{\alpha-1}(x,t) \quad (17)$$

512 Eq. (17) provides a recurrent relationship between the DSD moments of different orders. This  
 513 relationship was discussed by Pinsky et al.'s (2014) while analyzing diffusion growth in an  
 514 ascending adiabatic parcel.

515 In particular, the equation for the liquid water mixing ratio that is a moment of the order of

516  $\alpha = \frac{3}{2}$  can be written as

$$517 \quad \frac{\partial q(x,t)}{\partial t} = K \frac{\partial^2 q(x,t)}{\partial x^2} + \frac{4\pi\rho_w N(x,t)\bar{r}(x,t)}{F\rho_a} S(x,t) \quad (18)$$

518 where the mean radius  $\bar{r}(x,t) = \frac{m_{1/2}}{m_0}$ .

519 In the general case, Eq. (18) is not closed, since concentration  $N(x,t)$  and  $\bar{r}(x,t)$  are unknown  
 520 functions of time and spatial coordinates.

521 The characteristic time of evaporation and of supersaturation change is the phase relaxation  
 522 time (Korolev and Mazin, 2003)

$$523 \quad \tau_{pr} = \frac{\rho_a F}{4\pi\rho_w A_2 N \bar{r}} \quad (19)$$

524 Using Eq. (19), Eq. (18) can be rewritten as

$$525 \quad \begin{aligned} \frac{\partial q(x,t)}{\partial t} &= K \frac{\partial^2 q(x,t)}{\partial x^2} + \frac{1}{\tau_{pr}(x,t)} \left[ \frac{1}{A_2} \Gamma(x,t) - q(x,t) \right] = \\ &= K \frac{\partial^2 q(x,t)}{\partial x^2} + \frac{1}{A_2 \tau_{pr}(x,t)} S(x,t) \end{aligned} \quad (20)$$

526 From Eqs. (20) and (15), the equation for supersaturation can be written in the following simple  
 527 form

$$528 \quad \frac{\partial S(x,t)}{\partial t} = K \frac{\partial^2 S(x,t)}{\partial x^2} - \frac{S(x,t)}{\tau_{pr}(x,t)} \quad (20a)$$

529 Eqs. (20) and (20a) show that changes in the microphysical variables are determined by the rate  
 530 of spatial diffusion (the first term on the right-hand side of these equations) and of evaporation  
 531 (the second term on the right-hand side).

532

### 533 **3. Analysis of non-dimensional equations**

534 Spatial diffusion and evaporation depend on many parameters. It is the best to start the  
 535 analysis from the basic equation system presented in a non-dimensional form. A time scale  
 536 corresponding to the initial phase relaxation time in a cloud volume can be defined as

$$537 \quad \tau_0 = \frac{\rho_a F}{4\pi\rho_w A_2 N_1 r_0} \quad (21)$$

538 and the non-dimensional time is  $\tilde{t} = t / \tau_0$ . Other non-dimensional parameters to be used are:

539 the non-dimensional phase relaxation time

$$540 \quad \tilde{\tau}_{pr} = \tau_{pr} / \tau_0 = \frac{N_1 r_0}{N(\tilde{x}, \tilde{t}) \bar{r}(\tilde{x}, \tilde{t})}, \quad (22a),$$

541 **the normalized liquid water mixing ratio which is equal to the normalized liquid water content**

$$542 \quad \tilde{q} = \frac{q}{q_1}, \quad (22b),$$

543 the normalized supersaturation

$$544 \quad \tilde{S} = \frac{S}{A_2 q_1} \quad (22c),$$

545 the non-dimensional conservative function

$$546 \quad \tilde{\Gamma} = \frac{\Gamma}{A_2 q_1}, \quad (22d),$$

547 the normalized square of droplet radius

$$548 \quad \tilde{\sigma} = \frac{\sigma}{r_0^2}, \quad (22e),$$

549 the normalized droplet concentration

$$550 \quad \tilde{N} = N / N_1 \quad (22f)$$

551 and the non-dimensional DSD

$$552 \quad \tilde{g}(\tilde{\sigma}) = \frac{r_0^2}{N_1} g(\sigma) \quad (22g).$$

553 with normalization  $\tilde{N} = \int_0^1 \tilde{g}(\tilde{\sigma}) d\tilde{\sigma}$ . The definition (22g) means that the integral of a non-

554 dimensional initial size distribution over the normalized square radius is equal to unity.

555 The non-dimensional distance and the non-dimensional time are defined as

$$556 \quad \tilde{x} = x/L; \quad \tilde{t} = t/\tau_0 \quad (22h)$$

557 A widely used non-dimensional parameter showing the comparative rates of diffusion and  
558 evaporation is the Damkölher number:

$$559 \quad Da = \frac{\tau_{mix}}{\tau_0} = \frac{L^2}{K\tau_0} \quad (23)$$

560 where

$$561 \quad \tau_{mix} = \frac{L^2}{K} \quad (24)$$

562 is the characteristic time scale of mixing. Using the non-dimensional parameters listed above,

563 Eq. (20) can be rewritten in a non-dimensional form as

564

$$565 \quad \frac{\partial \tilde{q}(\tilde{x}, \tilde{t})}{\partial \tilde{t}} = \frac{1}{Da} \frac{\partial^2 \tilde{q}(\tilde{x}, \tilde{t})}{\partial \tilde{x}^2} + \frac{1}{\tilde{\tau}_{pr}(\tilde{x}, \tilde{t})} [\tilde{\Gamma}(\tilde{x}, \tilde{t}) - \tilde{q}(\tilde{x}, \tilde{t})] =$$

$$\frac{1}{Da} \frac{\partial^2 \tilde{q}(\tilde{x}, \tilde{t})}{\partial \tilde{x}^2} + \frac{1}{\tilde{\tau}_{pr}(\tilde{x}, \tilde{t})} \tilde{S}(\tilde{x}, \tilde{t}) \quad (25)$$

566 where

$$567 \quad \tilde{q}(\tilde{x}, \tilde{t}) = \frac{N(\tilde{x}, \tilde{t}) \overline{\sigma^{3/2}}}{N_1 r_0^3} = \int_0^\infty \tilde{\sigma}^{3/2} \tilde{g}(\tilde{x}, \tilde{t}, \tilde{\sigma}) d\tilde{\sigma} \quad (26)$$

568 The initial conditions and the boundary conditions should be rewritten in a non-dimensional

569 form as well. For instance, the normalized initial condition for the non-dimensional function

570  $\tilde{q}(\tilde{x}, 0)$  can be derived from Eqs. (1c) and (22b)

$$571 \quad \tilde{q}(\tilde{x}, 0) = \begin{cases} 1 & \text{if } 0 \leq \tilde{x} < 1/2 \\ 0 & \text{if } 1/2 \leq \tilde{x} < 1 \end{cases} \quad (27)$$

572 The solution for  $\tilde{\Gamma}(\tilde{x}, \tilde{t})$  obtained by a normalization of solution (7) is

$$573 \quad \tilde{\Gamma}(\tilde{x}, \tilde{t}) = \frac{1}{2}(1+R) + (1-R) \sum_{n=1}^{\infty} \frac{\sin(n\pi/2)}{n\pi/2} \exp\left(-\frac{n^2\pi^2\tilde{t}}{Da}\right) \cos(n\pi\tilde{x}), \quad (28)$$

574 where

$$575 \quad R = \frac{S_2}{A_2 q_1} \quad (29)$$

576 is a non-dimensional parameter referred to, hereafter, as a potential evaporation parameter  
 577 (PEP). The PEP is proportional to the ratio of the amount of water vapour that should  
 578 evaporate in order to saturate the initially droplet-free volume (that is determined by  $S_2$ ) to the  
 579 initial available liquid water  $q_1$  in the cloud volume. The solution of Eq. (28) at  $t \rightarrow \infty$  depends  
 580 only on parameter  $R$ .

$$581 \quad \tilde{\Gamma}(\tilde{x}, \infty) = \frac{1}{2}(1+R) \quad (30)$$

582 The importance of PEP that determines a possible final state was illustrated in Pt. 1. PEP is  
 583 also the sole parameter enabling calculation of the normalized mixing diagram for  
 584 homogeneous mixing (Pt. 2). In this study, we consider cases when  $R < 0$  since  $S_2 < 0$ , i.e.  
 585 when droplets can only evaporate in the course of mixing.

586 The solution of Eq. (25) and the type of mixing depends on the values of two non-  
 587 dimensional parameters, namely,  $Da$  and  $R$ . Thus, when  $R = \frac{S_2}{A_2 q_1} < -1$ ,  $\tilde{\Gamma}(\tilde{x}, \infty) < 0$ . It means  
 588 that the initially droplet-free volume  $V_2$  is too dry and all the droplets in the mixing volume  
 589 evaporate completely. At the final equilibrium state  $RH < 100\%$ , i.e.  $S(x, \infty) < 0$ . If

590  $R = \frac{S_2}{A_2 q_1} > -1$ ,  $\tilde{\Gamma}(\tilde{x}, \infty) > 0$ . This means that the mixed volume in the final state contains

591 droplets, i.e. the mixing leads expands the volume with droplets, i.e. the cloud volume. At the

592 final equilibrium state,  $RH = 100\%$  (i.e.  $S(x, \infty) = 0$ ). The case when  $|R| = \left| \frac{S_2}{A_2 q_1} \right| = |\tilde{S}_2| \ll 1$   
 593 corresponds to either  $RH$  close to 100% (i.e.  $S_2$  is close to zero) (this case corresponds to the  
 594 degenerated case considered in Pt. 1), and/or to the case when the liquid water mixing ratio in  
 595 the cloud volume is large. In case  $|R| \ll 1$ , the second term on the right-hand side of Eq. (25) is  
 596 much smaller than the first term, and the mixing is driven by turbulent diffusion only.

597 In case  $Da \rightarrow 0$  (often considered as homogeneous mixing), at the beginning of the mixing  
 598 the diffusion term is much larger than the evaporation term, the second term on the right-hand  
 599 side of Eq. (25). As mixing proceeds, within a short time period the total homogenization of all  
 600 the variables in the mixing volume is established and all the spatial gradients become equal to  
 601 zero. At this time instance, the first term on the right-hand side becomes equal to zero, and the  
 602 second term on the right-hand side of Eq. (25), describing droplet evaporation, becomes  
 603 dominant. Thus, the analysis of the Eq. (25) shows that mixing consists of two stages. The first  
 604 mixing stage is a short stage of inhomogeneous mixing and the longer second stage of  
 605 homogeneous mixing. The evolution of the microphysical variables during homogeneous  
 606 mixing is described in detail in Pt. 2.

607  $Da \rightarrow \infty$  corresponds to extremely inhomogeneous mixing, according to the classic  
 608 concept. In this case, the diffusion term is much smaller than the evaporation term, so  
 609 evaporation takes place under significant spatial gradients of  $RH$ . At  $Da = \infty$ , the adjacent  
 610 volumes do not mix at all and remain separated. This equivalent to existence of two  
 611 independent adiabatic volumes. Another interpretation of the limiting case  $Da = \infty$  is an  
 612 infinite fast droplet evaporation. Both scenarios at  $Da \rightarrow \infty$  indicate simplifications in the  
 613 definition of the extremely inhomogeneous mixing. At intermediate values of  $Da$ , mixing is  
 614 inhomogeneous, when both turbulent diffusion and evaporation contribute simultaneously to  
 615 formation of the DSD.



616 Using Eq. (14) and normalization (22f), the equations for the non-dimensional size  
 617 distribution can be written as

$$618 \quad \frac{\partial \tilde{g}(\tilde{x}, \tilde{t}, \tilde{\sigma})}{\partial \tilde{t}} = \frac{1}{Da} \frac{\partial^2 \tilde{g}(\tilde{x}, \tilde{t}, \tilde{\sigma})}{\partial \tilde{x}^2} + \frac{2}{3} [\tilde{\Gamma}(\tilde{x}, \tilde{t}) - \tilde{q}(\tilde{x}, \tilde{t})] \frac{\partial \tilde{g}(\tilde{x}, \tilde{t}, \tilde{\sigma})}{\partial \tilde{\sigma}} \quad (31)$$

619

620 Eq. (31) is solved with the following initial conditions

621

$$622 \quad \tilde{g}(\tilde{x}, 0, \tilde{\sigma}) = \begin{cases} \delta(\tilde{\sigma} - 1) & \text{if } 0 \leq \tilde{x} < 1/2 \\ 0 & \text{if } 1/2 \leq \tilde{x} \leq 1 \end{cases} \quad (32)$$

623 where  $\delta(\tilde{\sigma} - 1)$  is a delta function.

624

625 **Table 1** presents the list of all the non-dimensional variables used in this study and the  
 626 ranges of their variation. It is shown that six parameters determining the geometrical and  
 627 microphysical properties of mixing can be reduced to two non-dimensional parameters, which  
 628 enables a more efficient analysis of mixing. The ranges of parameter variations in Tab. 1  
 629 correspond to the simplifications used in the study (the initial DSD is monodisperse  
 630 and  $RH \leq 100\%$ ).

631

#### 632 **4. Design of simulations**

##### 633 ***Damköhler number $Da$ in clouds***

634 The characteristic mixing time  $\tau_{mix}$  can be evaluated using Eqs. (2) and (24)

$$635 \quad \tau_{mix} = \frac{1}{C} \varepsilon^{-1/3} L^{2/3} \quad (33)$$

636 There is significant uncertainty regarding the evaluation of  $\tau_{mix}$  and  $Da$  in clouds, which is  
 637 largely related to the choice of coefficient  $C$  in expression (33). These values differ in different  
 638 studies:  $C = 10$  (Jeffery and Reisner, 2006);  $C = 1$  (Lehmann et al., 2009) and  $C \approx 0.2$  (  
 639 Monin and Yaglom, 1975) and Boffetta and Sokolov (2002).

640 According to Lehmann et al. (2009), the values of  $Da$  in clouds of different types range  
 641 from to 0.1 to several hundred. Thus, estimation of  $Da$  in clouds may vary within a wide range  
 642 up to a few orders of magnitude.  $Da$  values of in stratocumulus clouds can be similar or even  
 643 higher than those in cumulus clouds, since both  $\tau_{mix}$  and  $\tau_{pr}$  in stratiform clouds are larger than  
 644 in cumulus clouds.

645 In our simulations, we compare the evolution of the microphysical parameters within a  
 646 wide range of  $Da$  (from 1 up to 500) and of  $R$  (from -1.5 up to -0.1).  $Da = 1$  represents the  
 647 case closest to homogeneous mixing, while  $Da = 500$  indicates extremely inhomogeneous  
 648 mixing.

649

### 650 ***Numerical method***

651 Calculations were performed using MATLAB solver PDEPE. We solve the equation  
 652 system (31) for normalized DSD  $\tilde{g}(\tilde{x}, \tilde{t}, \tilde{\sigma}_j)$  with the initial condition (32) and the Neumann  
 653 boundary conditions

654

$$655 \frac{\partial \tilde{g}(0, \tilde{t}, \tilde{\sigma}_j)}{\partial \tilde{x}} = \frac{\partial \tilde{g}(1, \tilde{t}, \tilde{\sigma}_j)}{\partial \tilde{x}} = 0 \quad (34)$$

656 where  $j = 1 \dots 24$  are the bin numbers on a linear grid of square radii. The number of grid points  
 657 along the  $\tilde{x}$  axis was set equal to 81.

658 In calculation of the last term on the right-hand side of Eq. (31), the normalized  
 659 supersaturation  $\tilde{S}$  was calculated first using the normalized conservative equation

$$660 \tilde{S}(\tilde{x}, \tilde{t}) = \tilde{\Gamma}(\tilde{x}, \tilde{t}) - \tilde{q}(\tilde{x}, \tilde{t}) \quad (35)$$

661 where  $\tilde{\Gamma}(\tilde{x}, \tilde{t})$  is calculated using Eq. (28). Then, this term was formulated using Eq. (9) as

$$662 \frac{2}{3} \tilde{S}(\tilde{x}, \tilde{t}) \frac{\partial \tilde{g}(\tilde{x}, \tilde{t}, \tilde{\sigma}_j)}{\partial \tilde{\sigma}_j} \approx \frac{\tilde{g}\left(\tilde{x}, \tilde{t}, \tilde{\sigma}_j + \frac{2}{3} \tilde{S} \Delta \tilde{t}\right) - \tilde{g}(\tilde{x}, \tilde{t}, \tilde{\sigma}_j)}{\Delta \tilde{t}} \quad (36)$$

663 Therefore, at each time step, the DSD  $\tilde{g}$  first was shifted to the left to the value  $\frac{2}{3}\tilde{S}\Delta\tilde{t}$ , where  
 664  $\Delta\tilde{t}$  is a small time increment chosen so that  $\left|\frac{2}{3}\tilde{S}_{\max}\Delta\tilde{t}\right| \leq \frac{\Delta\tilde{\sigma}}{2}$ . Next, the shifted DSD was  
 665 remapped onto the fixed square radius grid  $\tilde{\sigma}_j$ . We used the remapping method proposed by  
 666 Kovetz and Olund (1969), which conserves droplet concentration and LWC. After remapping,  
 667 the differences between the new and old DSDs were recalculated. The new values of LWC then  
 668 were determined using new values of DSD and Eq. (26). MATLAB utility PDEPE  
 669 automatically chooses the time step needed to provide stability of calculations.

670

## 671 **5. Results of simulations**

### 672 **5.1 Full evaporation case**

673 First, we consider the case  $R = -1.5$ , when all the cloud water evaporates completely. This  
 674 process corresponds to the cloud dissipation caused by mixing with the entrained dry air. At the  
 675 final state, RH is expected to be uniform and negative over the entire mixing volume.

676 **Figure 3** shows spatial and time changes of  $\tilde{S}$  for  $Da = 1, 50$  and  $500$ . At the final state  
 677 for all the three cases  $\tilde{S} = -0.25$ , which is in agreement with the analytical solution of Eq. (30).  
 678 The final negative value indicates that all the droplets completely evaporated during mixing. At  
 679  $Da = 1$  (Fig.3ab), two stages of supersaturation evolution can be identified. The first short  
 680 stage with  $t < 0.4\tau_{pr}$  is the period of inhomogeneous mixing, when the gradients of  $RH$   
 681 persist. By end of the second stage of about  $14\tau_{pr}$ , the equilibrium state is reached. Thus, at  
 682 small  $Da$  both types of mixing take place. In the cases of  $Da = 50$  and  $Da = 500$ , the spatial  
 683 gradients exit during the entire period of mixing until the equilibrium state is reached  
 684 (approximately  $50\tau_{pr}$  and  $300\tau_{pr}$ , respectively) (Fig.3cdef). Therefore, at these  $Da$  mixing is  
 685 inhomogeneous during entire mixing.

686 **Figure 4** shows spatial changes (upper row) and changes in  $\tilde{x}-\tilde{t}$  coordinates (lower row)  
 687 of normalized LWC for the same case as in Fig.3. These diagrams demonstrate a significant  
 688 difference in the evaporation rates at different  $Da$  values. Complete evaporation (LWC=0) is  
 689 reached at  $Da = 1, 50$  and  $500$  by about 12, 22 and 120 relaxation times periods , respectively.

690 Analysis of Figs. 3 and 4 allows to introduce two characteristic time periods: (1) period  $T_{mix}$   
 691 during which the spatial gradients of the microphysical parameters persist, and mixing is  
 692 inhomogeneous, and (2) period  $T_{ev}$  during which droplet evaporation takes place. Both time  
 693 periods are dimensionless and normalized using  $\tau_0$ . Time period  $T_{ev}$  is equal either to the time  
 694 of complete droplet evaporation (when  $R < -1.0$ ) or to the time period during which the  
 695 saturation deficit in the mixing volume becomes equal to zero (or close to zero if  $R > -1.0$ ),  
 696 i.e. evaporation is actually terminated. Quantitative evaluations of  $T_{mix}$  and  $T_{ev}$  will be given in  
 697 Section 5.3. At  $\tilde{t} < T_{mix}$ , droplets in the mixing volume experience different saturation deficits.  
 698 Toward the end of time  $T_{mix}$  the saturation deficit becomes uniform over the entire mixing  
 699 volume because of mechanic mixing. At  $Da = 1$ , the homogenization of the saturation deficit  
 700 and all the microphysical variables takes place during a very short time of about  $0.5\tau_{pr}$ , and  
 701 then the evaporation of droplets is assumed to take place under the same subsaturation  
 702 conditions, so  $T_{mix} \ll T_{ev}$ .

703 Figs. 4a,b show that at  $\tilde{t} \approx 0.35$ , normalized LWC drops down from 1 to 0.4. Since the  
 704 average value of the normalized LWC in the mixing volume is equal to 0.5 (see the initial  
 705 condition in Eq. (27)), 20% of the droplet mass evaporates during this short inhomogeneous  
 706 period. Thus, despite being quite short, inhomogeneous mixing stage plays an important role  
 707 even at  $Da = 1$ .

708 Since at  $t = 0$  the mixing volume is not spatially homogeneous by definition, there is  
 709 always a period while spatial inhomogeneity exists. With increasing  $Da$ , the duration of the  
 710 inhomogeneous stage increases and the duration of the homogeneous stage decreases. At

711  $Da = 500$ , homogenization of the saturation deficit requires  $250\tau_{pr}$ , which is twice as long as  
 712 the time of complete droplet evaporation, i.e.  $T_{mix} \approx 2T_{ev}$ . This means that at  $Da = 500$ , droplet  
 713 evaporation takes place in the presence of the spatial gradients of supersaturation. After  
 714 complete evaporation of droplets, spatial gradients of the water vapour mixing ratios remain.  
 715 This kind of mixing is regarded as inhomogeneous.

716 At  $Da = 50$ , the time of complete evaporation is approximately equal to the time of  
 717 supersaturation homogenization, i.e.  $T_{mix} \approx T_{ev}$ . In this case, as at  $Da = 500$ , the droplets  
 718 experience different saturation deficit within the mixing volume, so mixing is inhomogeneous  
 719 at  $Da = 50$ .

720 The differences in droplet evaporation at different  $Da$  can be seen in **Figure 5.**, showing  
 721 the relationships between  $\tilde{N}$  and  $\tilde{q}$  plotted with a certain time increment, so that each symbol  
 722 in the diagrams corresponds to a particular time instance. These symbols form curves. Each  
 723 panel of Fig. 5 shows three curves corresponding to different  $\tilde{x}$ : the centre of the initially cloud  
 724 volume ( $\tilde{x} = 1/4$ ); the centre of the mixing volume ( $\tilde{x} = 1/2$ ) and the centre of the initially  
 725 droplet-free volume ( $\tilde{x} = 3/4$ ). The directions of the time increase are shown by arrows along  
 726 the corresponding curves. The initial points of the curves corresponding to  $\tilde{t} = 0$  are  
 727 characterized by values  $\tilde{q} = 1$  and  $\tilde{N} = 1$  at  $\tilde{x} = 1/4$ , and by values  $\tilde{q} = 0$  and  $\tilde{N} = 0$  at  $\tilde{x} = 3/4$ .

728 The behaviour of the  $\tilde{N} - \tilde{q}$  relationship provides important information about mixing  
 729 process. At  $\tilde{t} < T_{mix}$ , there are spatial gradients of  $\tilde{N}$  and  $\tilde{q}$ , i.e.  $\tilde{N}$  and  $\tilde{q}$  are different at  
 730 different  $\tilde{x}$ . This means that the three curves at  $\tilde{t} < T_{mix}$  do not coincide. At  $\tilde{t} > T_{mix}$ , the spatial  
 731 gradients of  $\tilde{N}$  and  $\tilde{q}$  disappear and the three curves coincide. When the curves do not  
 732 coincide, mixing is inhomogeneous, and the coincidence of the curves indicates that the mixing  
 733 becomes homogeneous. In Fig. 5a and 5b ( $Da = 1$  and  $Da = 5$ , respectively), the curves  
 734 coincide at point A corresponding to time  $\tilde{t} = T_{mix}$ .

735 Figs. 5a,b show that at  $Da = 1$  and  $Da = 5$ , mixing consists of two stages: inhomogeneous  
 736 and homogeneous. The time instance  $\tilde{t} = T_{mix}$  separates these two stages. In turn, the period of  
 737 homogeneous mixing (when evaporation is spatially homogeneous) can be separated into two  
 738 sub-periods. During the first sub-period, droplets evaporate only partially and  $\tilde{q}$  decreases at  
 739 the same droplet concentration. This sub-period is very pronounced at  $Da = 1$ , when  $\tilde{q}$   
 740 decreases from about 0.4 to 0.1 at the unchanged droplet concentration. At the second sub-  
 741 period, when  $\tilde{q} < 0.1$ , droplets evaporate completely, beginning with smaller ones, so both the  
 742 droplet concentration and  $\tilde{q}$  rapidly drop to zero. At  $Da = 5$  (Fig. 5b), at the stage of  
 743 homogeneous evaporation (that begins at point “A”) the decrease in  $\tilde{q}$  is accompanied by a  
 744 decrease in  $\tilde{N}$ .

745 At  $Da = 50$  (Fig 5c), curves corresponding to different values of  $\tilde{x}$  do not coincide, except  
 746 at the final point “F”, where  $\tilde{N} = 0$  and  $\tilde{q} = 0$ . This means that horizontal gradients exist during  
 747 the entire mixing process and mixing is inhomogeneous till the final equilibrium state is  
 748 reached. Droplets penetrating into the initially droplet-free volume begin evaporating, so only a  
 749 small fraction of droplets reaches the centre of the droplet-free volume, as seen in Fig. 5c,  
 750  $\tilde{x} = 3/4$  (black curve). Accordingly, at  $\tilde{x} = 3/4$  the droplet concentrations and  $\tilde{q}$  reach their  
 751 maxima (of 0.1 and 0.05, respectively) and then decrease to zero. At  $Da = 500$  (Fig 5d), all  
 752 the droplets evaporate before reaching the centre of the dry volume, indicating an extremely  
 753 high spatial inhomogeneity of droplet evaporation. Hence, only two curves for  $\tilde{x} = 1/4$  and  
 754  $\tilde{x} = 1/2$  are seen in Fig.5d.

755 Fig. 5 also shows that the slopes of the curves describing the  $\tilde{N} - \tilde{q}$  relationships are  
 756 different at different values of  $\tilde{x}$  and change over time. At large  $Da$ , the slopes of the curves  
 757 describing the dependencies  $\tilde{N} - \tilde{q}$  in the initially cloud volume are close to linear. However,  
 758 the slope at a high value of  $\tilde{q}$  is still flatter than that at a low value of  $\tilde{q}$ . This can be attributed  
 759 to the fact that when  $\tilde{q}$  is large, it decreases faster than the concentration  $\tilde{N}$  because some

760 fraction of droplets evaporate only partially. At the end of the mixing when  $\tilde{q}$  is small,  $\tilde{N}$   
 761 decreases faster than  $\tilde{q}$ , because the droplet concentration is determined by the smallest  
 762 droplets, while  $\tilde{q}$  is determined by larger droplets.

763 As was discussed in Pt. 1, according to the classical concept of extremely inhomogeneous  
 764 mixing, the ratio  $q/N$  remains constant. For dimensionless  $\tilde{N}$  and  $\tilde{q}$ , the scattering points  
 765 should be aligned along the 1:1 line. Therefore, the closeness of particular cases to the classical  
 766 extremely inhomogeneous mixing can be evaluated by the deviation of the  $\tilde{N}-\tilde{q}$  curve from  
 767 the 1:1 line. One can see that at  $Da = 500$  the  $\tilde{N}-\tilde{q}$  relationship is closer to linear.

768 Despite the fact that at  $R < -1$  all the droplets within the mixing volume evaporate, it is  
 769 interesting to follow the DSD evolution during this process. **Figure 6** shows the time evolution  
 770 of a normalized DSD at  $Da = 1$  and  $Da = 50$ . One can see a substantial difference in the DSD  
 771 evolutions at different  $Da$ . At  $Da = 1$ , different DSDs are formed very rapidly at different  
 772 values of  $\tilde{x}$  (panel a). The widest DSD occurs at  $\tilde{x} = 1$ , i.e. at the outer boundary of the initially  
 773 droplet-free volume. This is natural, because the supersaturation deficit is the highest at  $\tilde{x} = 1$ .  
 774 At  $\tilde{t} > T_{mix} \approx 0.4$ , DSD become similar at all values of  $\tilde{x}$  (Fig.6b). The DSD width continues to  
 775 increase due to partial droplet evaporation. This time period corresponds to the horizontal  
 776 segment of the  $\tilde{N}-\tilde{q}$  relationship in Fig. 5a. Fig. 6c shows the DSD at the stage when a  
 777 decrease in LWC is accompanied by a decrease in number droplet concentration. The  
 778 corresponding point in the  $\tilde{N}-\tilde{q}$  diagram at this time instance is quite close to the point “F” at  
 779 which  $\tilde{N} = 0$  and  $\tilde{q} = 0$ .

780 At  $Da = 50$ , DSD are different at different  $\tilde{x}$  during the entire period of mixing. While  
 781 DSD at  $\tilde{x} > 0.5$  are wide and droplet evaporation is accompanied by a shift of DSD maximum  
 782 to smaller droplet radii (this feature is typically attributed to homogeneous mixing), the DSD  
 783 maximum at  $\tilde{x} < 0.5$  (the initially cloud volume) shifts toward smaller radii only slightly until  
 784  $\tilde{t} = 3.17$  (Fig. 6e). Further droplet evaporation either leads to a complete evaporation (at

785  $\tilde{x} \geq 0.5$ ) or shifts the DSDs to smaller droplet sizes (panel f). The maximum droplet  
 786 concentration takes place at  $\tilde{x} = 0$ . Fig. 6 shows that DSD shapes evolve substantially over  
 787 time, although the final state is characterized by complete droplet evaporation.

788

## 789 **5.2 Partial evaporation case**

### 790 **5.2.1 Evolution of the microphysical parameters at different values of $Da$ and $R$**

791 Here we consider the process of mixing at  $R > -1$ , i.e. when not all the droplets evaporate  
 792 completely. **Figure 7** shows the horizontal profiles of a normalized supersaturation at different  
 793  $Da$  and  $R$ . One can see that in all cases, the final state occurs when the equilibrium  
 794 supersaturation  $\tilde{S} = 0$  (RH=100%). However, this final value is reached quite differently  
 795 depending on  $Da$ . At  $Da = 1$ , rapid mixing leads to formation of spatially homogeneous  
 796 humidity and supersaturation during a time period of a fraction of  $\tau_{pr}$ . Then, supersaturation  
 797 within the mixing volume grows by evaporation of droplets, which are uniformly distributed  
 798 over the entire mixing volume. This process of homogeneous mixing was analyzed in detail in  
 799 Pt. 2.

800 At  $Da = 500$ , changes in supersaturation take place largely within the initially droplet-free  
 801 volume. RH in the initially cloud volume undergoes only small changes. This process agrees  
 802 well with the classical concept of extremely inhomogeneous mixing. However, a strong  
 803 gradient of supersaturation remains within the initially drop-free volume for a long time (tens  
 804 of  $\tau_{pr}$ ). At  $Da = 50$ , the situation is intermediate. Mixing is intensive enough to decrease RH  
 805 in the initially cloud volume, but spatially uniform RH is established within about  $5-10\tau_{pr}$ ,  
 806 increasing with an increase in  $|R|$ . After this time instance, mixing takes place according to the  
 807 homogeneous scenario.

808 **Figure 8** shows the horizontal profiles of normalized LWC at different  $Da$  and  $R$ . At the  
 809 same  $R$ , the final equilibrium values of LWC are identical, as follows from Eq. (30); LWC



810 decreases with an increase in  $|R|$ . At any  $Da$ , the decrease in the LWC in the cloud volume is  
 811 caused largely by diffusion of droplets from the cloud volume into the initially droplet-free  
 812 volume .

813 At  $Da = 500$ , evaporation in the cloud volume is small because  $\tilde{S}$  in these volumes is high  
 814 in cloud volumes during mixing (Fig. 7). At  $Da = 1$ , the process of spatial homogenization  
 815 takes place during fractions of  $\tau_{pr}$ , i.e.  $T_{mix} < 1$ . Then, during a relatively lengthy period of  
 816  $10\tau_{pr}$ , evaporation decreases LWC over the entire mixing volume, which is characteristic of  
 817 homogeneous mixing. At  $Da = 50$ , spatial homogenization takes place during about  $T_{mix} \approx 15$ .  
 818 This is a slightly shorter time than it takes to establish the final equilibrium stage  $T_{tot}$ . Different  
 819  $Da$ 's cases reach equilibrium at different times. The process of reaching a final uniform LWC  
 820 lasts for  $100\tau_{pr}$  at  $Da = 500$  and for about  $\tau_{pr}$  at  $Da = 1$ .

821 **Figure 9** shows the profiles of the normalized droplet concentrations at different  $Da$  and  
 822  $R$ . In contrast to LWC, the final concentration depends both on  $Da$  and  $R$ . Hence, profiles at  
 823 different  $Da$  can have different shapes at the same value of  $R$ . At  $R = -0.1$  (which corresponds  
 824 to high RH in the initially dry volume) none of the droplets evaporate, so the final normalized  
 825 droplet concentration is equal to  $\tilde{N} = 1/2$ . This means that all the droplets in the initially cloud  
 826 volume are now uniformly distributed between both mixing volumes. At larger  $|R|$ , i.e., at  
 827 lower RH in an initially droplet-free volume, some droplets evaporate completely. The final  
 828 concentration decreases with an increase in  $Da$ .

829 The physical interpretation of this dependence is clear. At low  $Da$ , fast mixing leads to  
 830 formation of a uniform RH throughout the entire mixing volume, and this affects all the  
 831 droplets. At high  $Da$ , RH in the initially droplet-free volume remains low for a long time,  
 832 and droplets that penetrate can evaporate. Therefore, the fraction of completely evaporated  
 833 droplets increases with  $Da$ : at  $R = -0.1$  there are no completely evaporated droplets at any  $Da$ .

834 At  $R = -0.3$  a decrease in the droplet concentration takes place only at  $Da = 500$ , and at  
 835  $R = -0.5$  the droplet concentration decreases already at  $Da \geq 50$ .

836 The comparative contributions of different factors in establishing the final states of mixing  
 837 are well seen in **Figure 10** presenting the relationships between normalized concentration and  
 838 normalized LWC at three values of  $\tilde{x}$ :  $1/4$  (centre of the cloudy volume),  $1/2$  and  $3/4$  (centre of  
 839 the initially dry volume) at  $R = -0.5$  and different values of  $Da$ . Fig. 10 is analogous to Fig. 5,  
 840 but plotted for  $R > -1$ .

841 At  $Da = 1$  the mixing is very fast, which leads to a rapid decrease in LWC and in the  
 842 droplet concentration in the initially cloud volume and to an increase of these quantities in the  
 843 initially droplet-free volume. As a result of the rapid mixing and homogenization, all the curves  
 844 coincide at point “A” (left panel). After this time instance, spatial homogeneous evaporation  
 845 takes place. Since at  $Da = 1$  only partial, but not total, droplet evaporation occurs, the droplet  
 846 concentration remains unchanged even while LWC decreases. At  $Da = 50$  and  $Da = 500$ , the  
 847 three curves coincide at the final point “F” only. At  $Da = 500$ , the relationship between the  
 848 droplet concentration and the mass becomes more linear (blue curve). The linear dependence is  
 849 consistent with the concept of extremely inhomogeneous mixing (see Pt1). Considerations  
 850 regarding the closeness of the  $\tilde{N} - \tilde{q}$  relationship to the line 1:1 as a measure of  
 851 inhomogeneity of mixing made at  $R < -1$  are also valid for  $R > -1$ .

852

### 853 **5.2.2 Evolution of DSDs and the DSD parameters**

854 **Figure 11** presents examples of the DSD evolution at the center of the initially cloud  
 855 volume ( $\tilde{x} = 1/4$ ) (upper row) and of the initially droplet-free volume ( $\tilde{x} = 3/4$ ) at  $R = -0.5$   
 856 and different values of  $Da$ . Several specific features of the DSD are notable. As a result of the  
 857 rapid mixing at  $Da = 1$  (left column), DSD become similar in both volumes already at  
 858  $t = 0.317\tau_{pr}$  (black lines). Further evolution is similar in both volumes and is characterized by  
 859 broadening of the DSD and its shifting and of the DSD toward smaller droplet sizes. This shift

860 means a decrease in the mass at constant droplet concentration, which is typical of  
 861 homogeneous mixing.

862 The initially monodisperse DSDs become polydisperse. The mechanism of the DSD  
 863 broadening at  $Da=1$  is illustrated in **Figure 12**, showing the DSD at the earlier,  
 864 inhomogeneous stage at different  $\tilde{x}$ . One can see that within very short periods when the  
 865 spatial gradient of saturation deficit exists, droplets entering the initially droplet-free volume  
 866 partially evaporate, reaching their minimal size at  $\tilde{x}=1$ . In this way, a polydisperse DSD  
 867 forms. As the mixing proceeds, DSD become spatially homogenized, as seen in the right panel  
 868 of Fig. 12.

869 At  $Da=50$  and  $Da=500$ , the DSD shapes substantially differ from those at  $Da=1$ .  
 870 There are two main differences: the peak of the distribution shifts only slightly (at  $Da=50$ ) or  
 871 does not shift at all (at  $Da=500$ ). At the same time, the DSD develops a long tail of small  
 872 droplets. Since the mixing rate at these values of  $Da$  is slow, droplets penetrating deeper into  
 873 the initially dry volume remain there for long time and get smaller. As a result, at moderate  
 874 and large  $Da$ , a polydisperse DSDs form with droplet sizes ranging from zero to 1. Formation  
 875 of a long tail of small droplets in case of inhomogeneous mixing was simulated in direct  
 876 numerical simulation (DNS) by Kumar et al. (2012), as well as by means of “the explicit-  
 877 mixing parcel model” (EMPM) (Krueger et al., 1997; Su et al., 1998; Schlüter, 2006).

878 **Figure 13** shows the spatial dependencies of the DSD dispersion (ratio of DSD r.m.s. width  
 879 and the mean radius) at different time instances and different values of  $Da$  and  $R$ . One can see  
 880 that the dispersion increases with an increase in  $Da$  and in  $|R|$ . This behavior can be accounted  
 881 for by the fact that the DSD broadening toward smallest droplet size increases with the increase  
 882 in  $Da$  and in  $|R|$ . The DSD dispersion increases with time and with an increase in  $\tilde{x}$ , i.e.  
 883 further into the initially droplet free volume. At the same time, spatial homogenization takes  
 884 place, so at the final state at  $R=-0.5$  the DSD dispersion reaches 0.11 at  $Da=1$  and about 0.2  
 885 at  $Da=50$  and  $Da=500$ .

886 Observed DSD dispersion in different clouds typically ranges from 0.1 to 0.4 (Khain et al.,  
 887 2000; Martin et al., 2004; Prabha et al., 2012) and can be caused the following factors: in-  
 888 cloud nucleation (e.g. Khain et al., 2000; Pinsky and Khain, 2002), spatial averaging along  
 889 aircraft traverses (Korolev, 1995) and non-symmetry in droplet nucleation/denucleation  
 890 (Korolev, 1995). As seen in Fig. 13, this dispersion may be also caused by mixing at cloud  
 891 edges at moderate and large  $Da$ . Hence, inhomogeneous mixing leads to DSD broadening.

892 The effective radius,  $r_{eff}$ , is an important DSD characteristic. According to the classical  
 893 concept,  $r_{eff}$  remains unchanged during extremely inhomogeneous mixing, whereas decreases  
 894 during homogeneous mixing. **Figure 14** shows spatial dependencies of  $r_{eff}$  at different time  
 895 instances and different values of  $Da$  and  $R$ . At  $R = -0.1$  (high RH in the surrounding volume)  
 896  $r_{eff}$  is similar for all values of  $Da$ . So, at high  $R$  (i.e., close to zero), the behaviour of  $r_{eff}$  does  
 897 not allow to distinguish between mixing types.

898 At a given  $R$ , the final  $r_{eff}$  increases with increasing  $Da$ . For instance, at  $R = -0.5$ ,  $r_{eff}$  at  
 899 the final state differs from the initial  $r_{eff}$  value by less than 6% at  $Da = 500$ , while at  $Da = 1$   
 900  $r_{eff}$  decreases by 20%. At moderate and high  $Da$ , large gradients of  $r_{eff}$  exist during the  
 901 mixing process. However, the gradient is high only in the initially droplet-free volume where  
 902  $r_{eff}$  decreases significantly due to the intense evaporation of droplets. Besides,  $r_{eff}$  growth very  
 903 rapidly in the initially droplet free volume, so at high  $Da$  during most of the mixing time  $r_{eff}$   
 904 within the mixing volume becomes close to the initial  $r_{eff}$  value in the cloudy volume.

905

### 906 **5.3 Delimitation between mixing types**

907 Typically, the  $Da$  value is used as a criterion for delimitation between mixing types.  
 908  $Da = 1$  is usually used as a boundary value separating homogeneous and inhomogeneous  
 909 mixing. As shown in Section 4, mixing always starts as inhomogeneous. In the course of

910 mixing, the initial spatial gradients decrease and the air volumes either become identical or  
 911 remain different. In the former case, the second mixing stage is homogeneous. If  
 912 inhomogeneity persists until the equilibrium state is established, mixing remains  
 913 inhomogeneous during the entire period. Both mixing stages can be characterized by duration,  
 914 change in the droplet concentrations or LWCs, and other quantitative characteristics. These  
 915 characteristics are functions of two non-dimensional parameters  $R$  and  $Da$ , which can be  
 916 calculated and used for delimitation between mixing types. Since mixing between volumes  
 917 may turn from inhomogeneous into homogeneous before reaching the equilibrium state, it is  
 918 necessary to use some quantitative criteria to delimit mixing types. Below, delimitation is  
 919 performed for  $R > -1$  which corresponds to partial evaporation of droplets by the end of  
 920 mixing.

921

### 922 **5.3.1. Characteristic time periods of mixing**

923 Three characteristic time periods of mixing are distinguished: a) mixing period  $T_{mix}$ , during  
 924 which spatial gradients are smoothening (may be also called the homogenization period); b)  
 925 period  $T_{ev}$  during which  $S < 0$  and droplets evaporate until saturation is reached and c) the total  
 926 mixing period  $T_{tot}$  that lasts until the final equilibrium stage is reached. In our analysis, all the  
 927 three periods are assumed dimensionless quantities.

928 We use solution (28) for conservative function  $\tilde{\Gamma}(\tilde{x}, \tilde{t})$  to define quantitatively time period  
 929  $T_{mix}$ . The deviation of the solution from its final value  $\Delta\tilde{\Gamma} = \tilde{\Gamma}(\tilde{x}, \tilde{t}) - \tilde{\Gamma}(\tilde{x}, \infty)$  at  $\tilde{t} \rightarrow \infty$  can be  
 930 approximately estimated using the first term of the series expansion as

$$931 \quad \left| \Delta\tilde{\Gamma} \right|_{\max} \approx \left| (1-R) \frac{\sin(\pi/2)}{\pi/2} \exp\left(-\frac{\pi^2 \tilde{t}}{Da}\right) \cos(\pi \tilde{x}) \right|_{\max} = \quad (37)$$

$$\quad (1-R) \frac{2}{\pi} \exp\left(-\frac{\pi^2 \tilde{t}}{Da}\right)$$

932 From Eq. (37) the estimation of  $T_{mix}$  can be written as

933

$$934 \quad T_{mix} = -\frac{Da}{\pi^2} \ln \left[ \frac{\pi}{2(1-R)} \left| \Delta \tilde{\Gamma} \right|_{\max} \right] \quad (38a)$$

935 Suppose the value of the maximum deviation is  $\left| \Delta \tilde{\Gamma} \right|_{\max} = 0.02$ . This is a small value  
 936 compared to the initial leap of function  $\tilde{\Gamma}$ , which is equal to  $1-R$ . At  $\left| \Delta \tilde{\Gamma} \right|_{\max} = 0.02$  the  
 937 duration of the non-homogeneous stage is evaluated as

$$938 \quad T_{mix} = -\frac{Da}{\pi^2} \ln \left[ \frac{0.01\pi}{1-R} \right] \quad (38b)$$

939

940 Several studies evaluate the evaporation time for droplets of a particular size using the  
 941 equation for diffusion growth (e.g. Lehmann et al., 2009). In our study, the evaporation time  
 942 duration  $T_{ev}$  is defined as the period during which the maximum deviation of supersaturation  
 943 from zero exceeds the small value chosen as  $\left| \Delta \tilde{S} \right|_{\max} = 0.02$ :

$$944 \quad \left| \tilde{S}(\tilde{x}, T_{ev}) \right| \leq \left| \Delta \tilde{S} \right|_{\max} = 0.02 \quad (39)$$

945

946 Although criterion (39) is rather subjective, it has an advantage over the criterion used by  
 947 Lehmann et al. (2009), as Eq. (32) characterizes evaporation of the droplet population taking  
 948 into account the simultaneous increase in supersaturation, but not of individual droplets of  
 949 particular size at constant  $S$  as in Lehmann et al. (2009).

950 At the end of the mixing, both the thermodynamic equilibrium and the diffusion  
 951 equilibrium are reached. Accordingly, the total time of mixing  $T_{tot}$  is evaluated as the  
 952 maximum of the two time periods needed to achieve equilibrium  $T_{tot} = \max \{ T_{mix}, T_{ev} \}$ . All the  
 953 three characteristic time periods are normalized on the phase relaxation time, and, therefore,  
 954 depend on the two non-dimensional parameters  $R$  and  $Da$ . The contours of the characteristic  
 955 time durations  $T_{mix}$ ,  $T_{ev}$  and  $T_{tot}$  in the  $Da-R$  diagrams are shown in **Figure 15**.

956 As follows from Eq. (38b),  $T_{mix}$  is proportional to  $Da$ . The dependence of  $T_{mix}$  on  $R$  is not  
 957 very strong, so  $T_{mix}$  slightly decreases with increasing  $R$ . This can be attributed to the fact that  
 958 the lower  $R$ , the smaller the initial inhomogeneity of function  $\tilde{\Gamma}$  and the shorter the time to  
 959 align this inhomogeneity is. At small  $Da$  (high rate of homogenization of the volume),  $T_{ev}$   
 960 depends largely on  $R$ . At large  $Da$ ,  $T_{ev}$  depends substantially on  $Da$ , since the evaporation  
 961 rate depends on the number of droplets that diffuse to drier parts of the mixing volume. A  
 962 comparison of Fig. 15c with Figs. 15a and 15b shows that at small  $Da$ , time  $T_{tot}$  is determined  
 963 by  $T_{ev}$ , while at large  $Da$ ,  $T_{tot}$  is determined by  $T_{mix}$ .

964

### 965 **5.3.2. Determination of boundaries between the mixing types on the $R - Da$ plane**

966 Several criteria can be proposed for delimitation between mixing types. We consider these  
 967 criteria for  $R > -1$ . As discussed above, mixing always starts as inhomogeneous and late either  
 968 become homogeneous or remains inhomogeneous till the final equilibrium state is established.  
 969 At small  $Da$ , the homogenization takes place during  $T_{mix} < T_{tot}$ . The value of time fraction  $\lambda_1$  of  
 970 the inhomogeneous stage can serve as a criterion for definition of homogeneous mixing. This  
 971 formula for the fraction can be written as

$$972 \lambda_1 = \frac{T_{mix}}{T_{tot}} \quad (40)$$

973 The case  $\lambda_1 \leq 0.5$ , most time the mixing takes place according the homogeneous scenario and  
 974 such regime is reasonable to regard as homogeneous mixing. If  $\lambda_1(R, Da)$  changes within the  
 975 range of  $0.5 < \lambda_1 \leq 1$ , mixing appears to be intermediate. The criterion (40) depends on the non-  
 976 dimensional parameters  $R$  and  $Da$ . **Figure 16a** shows the boundaries separating mixing types  
 977 on the  $Da - R$  plane. These boundaries separate all plane into several zones. At very small  $R$ ,  
 978 the duration of the phase transition is negligibly small. According to criterion (40), in this case  
 979 mixing should be considered inhomogeneous, irrespective of the  $Da$  value.

980 Another criterion of delimitation between mixing types can be determined from a  
 981 comparison of LWC variation rates due to different mechanisms. The mean normalized LWC  
 982 (which is equal to the mean normalized liquid water mixing ratio) can be written as integral

983  $\langle \tilde{q}(\tilde{t}) \rangle = \int_0^1 \tilde{q}(\tilde{x}, \tilde{t}) d\tilde{x}$ . The initial mean LWC is equal to  $\langle \tilde{q}(t=0) \rangle = \frac{1}{2}$ . The final equilibrium

984 LWC is equal to  $\langle \tilde{q}(t=\infty) \rangle = \frac{1}{2}(1+R)$  (Eq. (30)). The total amount of liquid water that

985 evaporates in the course of mixing can be quantified by the difference between these two

986 values  $\langle \tilde{q}(t=0) \rangle - \langle \tilde{q}(t=\infty) \rangle = -\frac{1}{2}R$ . The amount of liquid water evaporated in the course of the

987 first inhomogeneous mixing stage is calculated by the equation

988  $\langle \tilde{q}(t=0) \rangle - \langle \tilde{q}(T_{mix}) \rangle = \frac{1}{2} - \langle \tilde{q}(T_{mix}) \rangle$ . Hence, parameter  $\lambda_2$  which is a ratio of

989

$$990 \lambda_2 = \frac{\langle \tilde{q}(t=0) \rangle - \langle \tilde{q}(T_{mix}) \rangle}{\langle \tilde{q}(t=0) \rangle - \langle \tilde{q}(t=\infty) \rangle} = \frac{2\langle \tilde{q}(T_{mix}) \rangle - 1}{R} \quad (41)$$

991 can serve as another possible criterion for delimitation between mixing types. This ratio

992 characterizes the fraction of liquid water that evaporates at the initial inhomogeneous stage.

993 Condition  $\lambda_2 < 0.5$  in this case corresponds to homogeneous mixing, while condition

994  $0.5 \leq \lambda_2 < 1$  corresponds to intermediate mixing. We regard the case  $\lambda_2 = 1$  as inhomogeneous

995 mixing. Certainly, criterion  $\lambda_2$  depends on the non-dimensional parameters  $R$  and  $Da$ . Fig.

996 16b illustrates delimitation between mixing types on the  $Da-R$  plane according to criterion

997  $\lambda_2$ .

998 Comparison of Figs. 16a and 16b shows that both criteria lead to nearly similar separation

999 of the  $Da-R$  plane into three zones corresponding to homogeneous, intermediate and

1000 inhomogeneous mixing. At the same time, the boundaries separating these zones are different

1001 depending on the delimitation criterion used. Nevertheless, it can be concluded that mixing can



1002 be considered homogeneous at  $Da$  below 4-10 and  $R < -0.1$  and inhomogeneous at  $Da$   
 1003 exceeding several tens.

1004 Terms "inhomogeneous mixing" (Burner and Brenguier, 2007) and "extremely  
 1005 inhomogeneous mixing" (Lehmann et al., 2009; Gerber et al., 2008; Pt1) are used to denote the  
 1006 mixing regime when the relationship between the normalized values  $\tilde{N}$  and  $\tilde{q}$  is represented  
 1007 by a straight 1:1 line, which is equivalent to the constant mean volume radius (in some studies,  
 1008 the effective radius is used instead of the mean volume radius. According to the definition used  
 1009 in the present study, extremely inhomogeneous mixing is the limiting case of inhomogeneous  
 1010 mixing when  $Da \rightarrow \infty$ . Despite the fact that the extremely inhomogeneous mixing is only an  
 1011 idealization our approach allows to determine to what extent mixing can be considered to be  
 1012 close to this limiting case. The measure of inhomogeneity of mixing is the closeness of the  
 1013  $\tilde{N} - \tilde{q}$  relationship to the 1:1 straight line (see discussion above related to Figs. 5 and 10).

1014 **Figure 17a** shows r.m.s. distance between the  $\tilde{N} - \tilde{q}$  relationship and the 1:1 straight line,  
 1015 depending on  $Da$  and  $R$ . These dependences were calculated using the set of points  $\tilde{N}_i, \tilde{q}_i$   
 1016 uniformly distributed over spatial interval  $0 \div 1$  and time interval  $0 \div T_{tot}$ . The equation for

1017 estimation is  $\delta = \sqrt{\frac{1}{2M} \sum_{i=1}^M (\tilde{N}_i - \tilde{q}_i)^2}$ , where  $M$  is the total number of points. This distance

1018 corresponds to r.m.s. deviation of the normalized mean volume radius from 1. The dependences  
 1019 of the last deviation on  $Da$  and  $R$  and estimated as  $\delta/3$  are shown in Fig. 17b. This estimation  
 1020 is based on the fact that the total mass of droplets is proportional to the cube of the mean  
 1021 volume radius. As expected, the distance decreases with increasing in  $Da$ . At large  $R$ , all the  
 1022 curves coincide indicating a degenerative case when type of mixing becomes indistinguishable.

1023 We choose the value  $\delta/3$  equal to 0.02 to determine the boundary of the extremely  
 1024 inhomogeneous mixing zone. The value of 0.02 corresponds to droplet radii deviation of a few  
 1025 tenths of a micron, which is so low that in in-situ measurements this case would always be  
 1026 attributed to extremely inhomogeneous mixing. In Fig.16 this boundary is marked by broken

1027 line. The boundary shows that the mixing at  $Da$  exceeding several hundred can be attributed  
 1028 to the extremely inhomogeneous. Between the boundary separating inhomogeneous mixing  
 1029 from the intermediate one and the boundary separated inhomogeneous mixing from extremely  
 1030 inhomogeneous there exists a wide zone of inhomogeneous mixing where the mean volume (or  
 1031 the effective) radius may drop by 10% and more (Fig. 14), and where the DSD dispersion is  
 1032 substantial and the tail of small droplets is long enough (Fig. 11). Mixing diagrams currently  
 1033 used for analysis of observed data ( $N-q$  dependences in the final equilibrium state of mixing)  
 1034 do not contain this zone which, therefore, has remained unrecognized and uninvestigated.

1035

## 1036 **6. Summary and conclusions**

1037 In this study, inhomogeneous turbulent mixing is investigated using a simple a 1D model of  
 1038 mixing between a saturated cloud volume and an undersaturated droplet-free volume. The  
 1039 mixing is simulated by solving a diffusion-evaporation equation written in the non-dimensional  
 1040 form. For simplicity, the initial volumes of cloudy and droplet-free air were assumed to be  
 1041 equal, and the initial DSD in the cloudy volume was assumed monodisperse.

1042 Analysis of the diffusion-evaporation equation shows that the time-dependent process of  
 1043 mixing and the final equilibrium state depend on two non-dimensional parameters. The first  
 1044 parameter  $R$ , referred in this paper as potential evaporation parameter (PEP) is proportional to  
 1045 the ratio between the saturation deficit in the initially droplet-free volume and the initial liquid  
 1046 water content in the cloudy volume. At  $R < -1$ , the final state is characterized by complete  
 1047 droplet evaporation and a spatially homogeneous saturation deficit, which indicates dissipation  
 1048 of the cloudy volume. At  $R > -1$ , the final state is characterized by existence of droplets and  
 1049 zero saturation deficit (RH=100%). In this case, the cloud volume expands after mixing with the  
 1050 entrained air. At small values of  $|R|$  (e.g., when RH in the entrained volume is close to 100%),  
 1051 the effect of droplet evaporation on microphysics is small, and, formally, this kind of mixing  
 1052 should be regarded as extremely inhomogeneous. Strictly speaking, this is a degenerate case,

1053 when homogeneous and inhomogeneous mixing cannot be distinguished (see also Pt. 1). At  
 1054  $R = 0$ , the droplet population turns into a passive admixture and its turbulent diffusion will be  
 1055 the same as different thermodynamic parameters.

1056 The second parameter is the *Damköhler* number ( $Da$ ) which is the ratio between the  
 1057 characteristic mixing time and the phase relaxation time. This parameter compares the rates of  
 1058 spatial diffusion and evaporation. Parameter  $Da$  (Eq. (23)) is logically appears in the non-  
 1059 dimensional form of the diffusion-evaporation equation showing that  $Da$  is the ratio of the  
 1060 mixing time defined as  $\tau_{mix} = \frac{L^2}{K}$ , to the initial drop relaxation time. The expression for this non-  
 1061 dimensional parameter clearly shows that since we consider an ensemble of evaporating droplets,  
 1062 the drop relaxation time evaluated just before the mixing is the characteristic time scale of  
 1063 inhomogeneous mixing process. In several studies (e.g., Baker and Latham, 1979; Burnet and  
 1064 Brenguier, 2007; Andejchuk et al., 2009) a question was raised as to which time scale should be  
 1065 used in formulation of the *Damköhler* number: the time of an individual droplet evaporation at  
 1066 constant saturation deficit, or the phase relaxation time. This study, as well Pt. 2 show that the  
 1067 phase relaxation time is the answer. The mixing time is introduced via the turbulent diffusion  
 1068 coefficient which is a natural measure characterizing the diffusion rate and, in particular,  
 1069 determines the propagation rate of the fronts in the fields of droplet concentration and other  
 1070 microphysical parameters. The turbulent diffusion coefficient is widely used to describe mixing  
 1071 in cloud models at resolved scales.

1072 The analysis was performed within a wide range of  $Da$  (from 1 to 500) and of  $R$  (from -  
 1073 1.5 to -0.1). The final LWC and the humidity in the mixing volume are determined by the mass  
 1074 conservation and do not depend on  $Da$  (see also Pt. 1 and Pt. 2). At the same time, the droplet  
 1075 concentration, as well as the shape of DSD and their parameters strongly depend on  $Da$ .

1076 It is shown that the mixing of air volumes with initially different thermodynamical and  
 1077 microphysical parameters consists of two stages characterized by two time periods: the time

1078 during which microphysical characteristics become uniform over the total mixing volume  $T_{mix}$ ,  
 1079 and the time during which zero saturation deficit is reached (at  $R > -1$ ),  $T_{ev}$ . At  $\tilde{t} < T_{mix}$ , the  
 1080 spatial gradients of the microphysical values remain and the mixing regime can be regarded as  
 1081 inhomogeneous. At  $\tilde{t} > T_{mix}$ , droplet evaporation, if it occurs at all, takes place within a  
 1082 spatially homogeneous medium, so all the droplets in the mixing volume experience equal  
 1083 saturation deficit. This regime can be regarded as homogeneous. It is shown, therefore, that at  
 1084 small  $Da$  mixing between two volumes that starts as inhomogeneous can become  
 1085 homogeneous towards the end of mixing.

1086 This finding allows to delimit between mixing types. We presented two quantitative criteria  
 1087 on the  $Da-R$  plane that allow to delimit three mixing regimes: homogeneous, intermediate  
 1088 and inhomogeneous. These criteria are based on comparison of the characteristic duration  
 1089 mixing and the evaporation rates. According to the criteria, at  $Da$  below about 5, mixing can  
 1090 be regarded as homogeneous, i.e. the main microphysical changes take place during the  
 1091 homogeneous stage. At  $5 < Da < 30 \div 50$ , the changes in the microphysical parameters are  
 1092 more significant at the inhomogeneous stage than at the homogeneous stage. In this case, the  
 1093 mixing can be regarded as intermediate. Finally, at  $Da$  exceeding several tens, the spatial  
 1094 microphysical gradients remain until the final equilibrium stage is reached. In this case, the  
 1095 mixing can be regarded as inhomogeneous. At  $Da$  exceeding a few hundred the deviations  
 1096 from predictions based of the classical concept of extremely inhomogeneous become relatively  
 1097 small, which justifies attribute regarding this mixing as extremely inhomogeneous.

1098 On the whole, the results of the present study are in line with the classic concepts defining  
 1099 homogeneous and inhomogeneous mixing types. However, several important points emerge  
 1100 from our work show serious limitations of classical concepts. A comparison of the classical  
 1101 concepts and the present study is presented in **Table 2**. Analysis of Tab. 2 shows the following.

1102 a) In contrast to many studies that analyze only the hypothetical final (equilibrium) state of  
 1103 mixing (Barnet and Brenguier, 2007; Gerber et al., 2008; Morrison and Grabowski, 2008; Hill

1104 et al., 2009), we consider the entire time-dependent processes of mixing and evaporation. At  
 1105 moderate and high  $Da$ , the mixing can last several minutes. In in-situ observations, we see  
 1106 mostly non-equilibrium stages which may account for a rather wide scattering of mixing  
 1107 diagrams even at the same values of  $Da$  (e.g., Lehmann et al., 2009).

1108 Note that time dependent mixing was also considered in several studies (e.g. Baker et al.,  
 1109 1980; Baker and Latham, 1982; Jeffery and Reisner, 2006; Krueger et al., 1997; Kumar et al.,  
 1110 2012) using different approaches and numerical models. These studies, however, do not contain  
 1111 analysis on non-dimensional diffusion-evaporation equation.

1112 b) It is also shown in the study that the slopes of the  $\tilde{N} - \tilde{q}$  relationship (between the  
 1113 normalized droplet concentration and LWC) tends to the 1:1 line with increasing  $Da$ . The  
 1114 closeness can be considered as a measure of extremely inhomogeneous mixing in terms of the  
 1115 classical concept (see Pt. 1). It has been found that the slope of the  $\tilde{N} - \tilde{q}$  relationship depends  
 1116 on the LWC and, accordingly, on time. At large LWC,  $\tilde{q}$  changes with time faster than  $\tilde{N}$ ,  
 1117 while at low LWC the concentration changes faster. Although mixing types are usually  
 1118 separated into homogeneous and extremely inhomogeneous, we have shown that there are wide  
 1119 ranges of  $Da$  and  $R$  at which mixing should be considered intermediate or inhomogeneous,  
 1120 but not extremely inhomogeneous. Within these ranges the effective radius can change by more  
 1121 than 10-15%. Standard mixing diagrams do not include this range that, to our knowledge, has  
 1122 never been investigated despite the fact that multiple in-situ measurements indicate its  
 1123 existence .

1124 c) Many studies assume the existence of pure homogeneous mixing during which the  
 1125 initially monodisperse DSD remains monodisperse. Our study shows that at the very beginning,  
 1126 mixing is always inhomogeneous. This inhomogeneous stage leads to formation of a  
 1127 polydisperse DSD that broadens in the course of droplet evaporation. Hence, even at  $Da = 1$   
 1128 the initially monodisperse spectrum becomes polydisperse.

1129 d) It is shown that at small  $Da$ , mixing includes both inhomogeneous and homogeneous  
1130 stages, which means that type of mixing can change during the mixing process.

1131 e) The classical concept assumes that the effective radius always decreases during  
1132 homogeneous mixing. Assuming an initially monodisperse DSD, we have found this  
1133 conclusion largely valid, with the exception small  $R$ . At the same time, it was shown in Pt. 2  
1134 that during homogeneous mixing, the effective radius can decrease, remain constant or increase  
1135 depending of the initial DSD shape. Thus, a decrease in the effective radius during mixing  
1136 cannot always be considered an indication of homogeneous mixing. Similarly, the invariability  
1137 the effective radius during mixing in the process cannot always be considered an indication of  
1138 extremely inhomogeneous mixing.

1139 f) It is generally assumed that during homogeneous mixing droplet concentration remains  
1140 unchanged. In the present study, as well as in Pt. 2, it is shown that since mixing leads to a  
1141 polydisperse DSD, the smallest droplets may completely evaporate. At  $R < -1$ , the DSD  
1142 becomes very wide and all the droplets, the smallest ones first, evaporate.

1143 g) It is generally assumed that inhomogeneous mixing does not alter DSD shape, but only  
1144 decreases droplet concentration. The present study showed that inhomogeneous mixing  
1145 significantly changes the DSD shape. DSD were found to be quite different in different regions  
1146 of mixing volumes. The main feature is the DSD broadening toward small droplet size, so the  
1147 relative dispersion grows up to 0.2-0.3. These values are quite close to those observed in  
1148 atmospheric clouds (Khain et al., 2000). Elongated tails of small droplets during mixing were  
1149 simulated by Schlüter (2006) who described turbulent diffusion following to Kruger et al.,  
1150 (1997) and Su et al., (1998) as well as by Kumar et al. (2012) using DNS. We see that  
1151 formation of a polydisperse DSD is a natural result of inhomogeneous mixing and, therefore,  
1152 inhomogeneous mixing is an important mechanism of DSD broadening. A significant impact  
1153 of mixing on DSD shape was found identified in multiple studies, beginning with Warner  
1154 (1973).

1155 h) The effective radius has been assumed to remain constant during extremely  
1156 inhomogeneous mixing. Our results indicate that, indeed, at the final equilibrium stage at  
1157 comparatively high RH the effective radius is close to that in the initially cloudy volume  
1158 (especially at high  $Da$ ). At the same time, we found that the effective radius varies in size and  
1159 is smaller in the initially droplet-free volumes.

1160 The results obtained in parts Pt1 and Pt 2, and especially in the current study (Pt 3)  
1161 dedicated to analysis of turbulent mixing mechanisms in clouds determine the directions for  
1162 future work. Since the widely used mixing diagrams show only a hypothetical equilibrium  
1163 state, but not the instantaneous state of mixing that likely correspond to transition periods, the  
1164 efficiency of the standard mixing diagrams is questionable. Moreover, the standard diagrams  
1165 miss a very important mixing regime, namely, inhomogeneous mixing that occurs between two  
1166 limiting cases of homogeneous and extremely inhomogeneous mixing (Fig. 16).

1167 We believe that the results obtained will help to improve understanding and interpretation  
1168 of mixing process both in in-situ measurements and modeling. The approach allows to  
1169 investigate the relationship between the main microphysical parameters typical of  
1170 inhomogeneous mixing, that differ from those in the limiting cases of extremely  
1171 inhomogeneous mixing. In addition, utilization of polydisperse DSD when solving diffusion-  
1172 evaporation equation allows to investigate the role of the initial DSD shape in mixing. In-situ  
1173 measurements (e.g., Burnet and Brenguier, 2007; Gerber et al., 2008; Lehmann et al., 2009)  
1174 and numerical models (Magaritz-Ronen et al., 2016) show a wide scattering of data on the  
1175 scattering diagrams. We expect location of various points on the diagrams (e.g.  $r_v^3$  vs. dilution  
1176 rates) depends on the shape of the initial DSDs and characterizes the stage of mixing. The  
1177 method applied in the study allows investigation of evolution of DSD moments over space and  
1178 time .

1179 Recently, there has been vigorous discussions concerning the possible existence of high  
1180 humidity layer near cloud edges that might affect mixing of cloud with its surrounding (Gerber

1181 et al., 2008; Lehmann et al., 2009). In our opinion, this layer does exist and forms as a result of  
1182 turbulent mixing of cloud with surrounding dry air, accompanied by complete droplet  
1183 evaporation. The approach developed in the present paper allows to analyze formation of such  
1184 humid layers.

1185 We believe that the results obtained in this study will foster the development of physically  
1186 grounded parameterization of mixing in cloud models.

1187

### 1188 *Acknowledgements*

1189 This research was supported by the Israel Science Foundation (grant 1393/14), the Office of  
1190 Science (BER), the US Department of Energy Award DE-SC0006788 and the Binational US-  
1191 Israel Science Foundation (grant 2010446). Dr. Korolev's participation was supported by  
1192 Environment Canada.

1193

1194

### 1195 **Appendix. List of symbols**

1196

1197 **Table A here**

1198

1199

1200

1201

1202

1203

1204

1205



1206

1207 **References**

1208 Andrejczuk M., W. Grabowski, S. P. Malinowski, P. K. Smolarkiewicz, 2009: Numerical

1209 Simulation of Cloud–Clear Air Interfacial Mixing: Homogeneous versus Inhomogeneous

1210 Mixing. *J. Atmos. Sci.*, **66**, 2993-2500.1211 Baker, M., and J. Latham: The evolution of droplet spectra and the rate of production of  
1212 embryonic raindrops in small cumulus clouds. *J. Atmos. Sci.*, **36**, 1612–1615, 1979.1213 Baker, M., R. G. Corbin, and J. Latham: The influence of entrainment on the evolution of  
1214 cloud drop spectra: I. A model of inhomogeneous mixing. *Quart. J. Roy. Meteor. Soc.*, **106**, 581–  
1215 598, 1980.1216 Baker M. B. and J. Latham: A diffusive model of the turbulent mixing of dry and cloudy  
1217 air *Quart. J. R. Met. Soc.*, **108**, 871-898, 19821218 Burnet, F., and J.-L. Brenguier, Observational study of the entrainment-mixing process in  
1219 warm convective cloud, *J. Atmos. Sci.*, 64, 1995–2011, 2007.1220 Blyth, A. M., Choularton, T. W., Fullarton, G., Latham, J., Mill, C. S., Smith, M. H., and  
1221 Stromberg, I. M.: The Influence of entrainment on the evolution of cloud droplet spectra. 2.  
1222 Field experiments 5 at Great Dun Fell, *Q. J. Roy. Meteor. Soc.*, **106**, 821–840, 1980.1223 Boffetta G. and I. M. Sokolov: relative dispersion in fully developed turbulence: The  
1224 Richardson’s law and intermittency correction. *Phys. Rev. Let.*, **88**, 094501, 2002.1225 Denvich B. J., P. Bartello, J.-L. Brenguier, L.R. Collins, W.W. Grabowski, R.H.A.  
1226 Ijzermans, S.P. Malinowski, M.W. Reeks, J.C. Vassilicos, L-P. Wang, and Z. Warhaft: Droplet  
1227 growth in warm turbulent clouds. *Q. J. Roy. Meteorol. Soc.*, **138**, 1401-1429, 20121228 Gerber H, Frick G, Jensen J.B, and Hudson J.G.: Entrainment, mixing, and microphysics in  
1229 trade-wind cumulus. *J. Meteorol. Soc. Jpn.*, **86A**. 87-106, 2008.

- 1230 Hill, A. A., G. Feingold, and H. Jiang: The Influence of Entrainment and Mixing  
1231 Assumption on Aerosol–Cloud Interactions in Marine Stratocumulus. *J. Atmos. Sci.*, **66**, 1450–  
1232 1464, 2009.
- 1233 Jeffery, C.A., and J.M. Reisner: A study of cloud mixing and evolution using PDF methods.  
1234 Part I: Cloud front propagation and evaporation. *J. Atmos. Sci.*, **63**, 2848-2864, 2006.
- 1235 Khain, A. P., M. Ovchinnikov, M. Pinsky, A. Pokrovsky, and H. Krugliak: Notes on the  
1236 state-of-the-art numerical modeling of cloud microphysics. *Atmos. Res.* **55**, 159-224, 2000.
- 1237 Korolev, A.V.: The influence of supersaturation fluctuations on droplet size spectra  
1238 formation. *J. Atmos. Sci.*, **52**, 3620-3634, 1995.
- 1239 Korolev A., and I. Mazin: Supersaturation of water vapor in clouds, *J. Atmos. Sci.*, **60**,  
1240 2957-2974, 2003.
- 1241 Korolev A., A. Khain, M. Pinsky, and J. French: Theoretical study of mixing in liquid  
1242 clouds. Part 1: classical concept. *Atmos. Chem. Phys.* , 2015 (submitted)
- 1243 Kovetz, A., and B. Olund: The effect of coalescence and condensation on rain formation in  
1244 a cloud of finite vertical extent. *J. Atmos. Sci.*, **26**, 1060–1065, 1969.
- 1245 Krueger S., C.-W. Su and P. McMurry: Modeling entrainment and finescale mixing in  
1246 cumulus clouds. *J. Atmos. Sci.*, **54**, 2697-2712, 1997
- 1247 Kumar B., F. Janetzko, J. Schumacher, and R. A. Shaw: Extremely responses of a coupled  
1248 scalar-particle system during turbulent mixing. *New J. of Phys.* **14**, 115020 , 2012
- 1249 Latham, J. and Reed, R. L.: Laboratory studies of effects of mixing on evolution of cloud  
1250 droplet spectra, *Q. J. Roy. Meteor. Soc.*, **103**, 297–306, 1977.
- 1251 Lehmann, K., H. Siebert, and R. A. Shaw: Homogeneous and inhomogeneous mixing in  
1252 cumulus clouds: Dependence on local turbulence structure. *J. Atmos. Sci.*, **66**, 3641-3659, 2009.
- 1253 Magaritz-Ronen L., A. Khain and M. Pinsky, 2016: About the Horizontal Variability of  
1254 Effective Radius in Stratocumulus Clouds. *J. Geophys. Res.* (in revision)

- 1255 Martin G.M., D. W. Johnson and A. Spice: The measurements and parameterization of  
 1256 effective radius of droplets in warm stratocumulus clouds. *J. Atmos. Sci.*, **51**, 1823-1842, 1994.
- 1257 Monin, A.S. and Yaglom, A.M.: “Statistical Fluid Mechanics: Mechanics of Turbulence”,  
 1258 vol. **2**, MIT Press. 1975
- 1259 Morrison, H., and W. W. Grabowski: Modeling supersaturation and subgrid-scale mixing  
 1260 with two-moment bulk warm microphysics. *J. Atmos. Sci.*, **65**, 792–812, 2008.
- 1261 Pinsky, M. and A. P. Khain: Effects of in-cloud nucleation and turbulence on droplet  
 1262 spectrum formation in cumulus clouds. *Quart. J. Roy. Meteorol. Soc.*, **128**, 1–33, 2002.
- 1263 Pinsky M., I. P. Mazin, A. Korolev, and A. Khain: Supersaturation and diffusional droplet  
 1264 growth in liquid clouds. *J. Atmos. Sci.*, **70**, 2778-2793, 2013.
- 1265 Pinsky M., I. P. Mazin, A. Korolev and A. Khain: Supersaturation and diffusional droplet  
 1266 growth in liquid clouds: Polydisperse spectra. *J. Geophys. Res., Atmospheres*, **119**, 12,872–  
 1267 12,887, 2014.
- 1268 Pinsky, M., Khain, A., Korolev, A., and Magaritz-Ronen, L.: Theoretical study of mixing in  
 1269 liquid clouds. Part 2: Homogeneous mixing. *Atmos. Chem. Phys.*, , 2016 (submitted)
- 1270 Polyanin A. D. and V. F. Zaitsev: Handbook of nonlinear partial differential equations.  
 1271 Chapman & Hall/CRC, 809 pp. , 2004
- 1272 Prabha V. T., S. Patade, G. Pandithurai, A. Khain, D. Axisa, P. Pradeep Kumar, R. S.  
 1273 Maheshkumar, J. R. Kulkarni, and B. N. Goswami: Spectral width of premonsoon and  
 1274 monsoon clouds over Indo-Gangetic valley during CAIPEEX, *J. Geop. Res.* **117**, D20205,  
 1275 doi:10.1029/2011JD016837 , 2012
- 1276 Pruppacher, H.R., Klett, J.D.. Microphysics of Clouds and Precipitation. 2nd edn. Oxford  
 1277 Press, 914 p. , 1997
- 1278 Rogers R. R. and Yau M. K: A Short Course in Cloud Physics, Pergamon press. 293pp. ,  
 1279 1989

1280 Schlüter M. H.: The effects of entrainment and mixing process on the droplet size  
1281 distribution in cumuli. A thesis submitted to the faculty of The University of Utah in partial  
1282 fulfillment of the requirements for the degree of Master of Science, Department of  
1283 Meteorology, The University of Utah, 92 pp., 2006

1284 Su C.-W., S.K. Krueger, P.A. McMurry and P.H. Austin: Linear eddy modeling of droplet  
1285 spectral evolution during entrainment and mixing in cumulus clouds. *Atmos. Res.*, **47-48**, 41-  
1286 58, 1998.

1287 Telford, J.W., and S. K. Chai: A new aspect of condensation theory. *Pageoph*, **118**, 720-  
1288 742 , 1980

1289 Warner, J.: The microstructure of cumulus cloud. Pt. I, General features of the droplet  
1290 spectrum, *J. Atmos. Sci.*, **26**, 1049-1059, 1969.

1291 Warner, J.. The microstructure of cumulus cloud: Part 4: The effect on the droplet spectrum  
1292 of mixing between cloud and environment. *J. Atmos. Sci.* **30**, 256–261, 1973.

1293

1294

1295

1296

1297

1298

1299

1300

1301

1302

1303

1304

1305

1306

1307 **Table 1. Main parameters of the problem and their non-dimensional forms\***

1308

Quantity	Symbol	Non-dimensional form	Range of normalized values
<b>Time</b>	$t$	$\tilde{t} = \frac{t}{\tau_0}$	$[0 \dots \infty]$
<b>Distance</b>	$x$	$\tilde{x} = \frac{x}{L}$	$[0 \dots 1]$
<b>Square of drop radius</b>	$\sigma$	$\tilde{\sigma} = \frac{\sigma}{r_0^2}$	$[0 \dots 1]$
<b>Droplet concentration</b>	$N$	$\tilde{N} = \frac{N}{N_1}$	$[0 \dots 1]$
<b>Liquid water mixing ratio</b>	$q$	$\tilde{q} = \frac{q}{q_1}$	$[0 \dots 1]$
<b>Distribution of square of drop radius</b>	$g(\sigma)$	$\tilde{g}(\tilde{\sigma}) = \frac{r_0^2}{N_1} g(\sigma)$	
<b>Conservative function</b>	$\Gamma$	$\tilde{\Gamma} = \frac{\Gamma}{A_2 q_1}$	$[-\infty \dots 1]$
<b>Supersaturation</b>	$S$	$\tilde{S} = \frac{S}{A_2 q_1}$	$[-\infty \dots 0]$
<b>Relaxation time</b>	$\tau_{pr}$	$\tilde{\tau}_{pr} = \frac{\tau_{pr}}{\tau_0}$	$[1 \dots \infty]$
<b>Damkölher number</b>	$Da$	$Da = \frac{\tau_{mix}}{\tau_0} = \frac{L^2}{K \tau_0}$	$[0 \dots \infty]$
<b>Potential evaporation parameter (PEP)</b>	$R$	$R = \frac{S_2}{A_2 q_1}$	$[-\infty \dots 0]$

1309

1310 \*All normalized values depend on the initially given values of  $L$ ,  $N_1$ ,  $r_0$ ,  $A_2$ ,  $S_2$  and  $K$ 

1311

1312

1313 **Table 2.** Comparison of analysis based on the classic concepts of mixing and the results of

1314 the present study

1315

Classical concept	The present study
Only the final equilibrium state is typically analyzed; results of in-situ observations are interpreted assuming the equilibrium state.	The mixing period can last several minutes and more. The microphysical structure of the mixing volumes during this period can differ substantially from that at the final state
Types of mixing are separated into homogeneous and extremely inhomogeneous.	There are the wide ranges of $Da$ and $R$ values, at which mixing can be regarded as intermediate or inhomogeneous (but not extremely inhomogeneous).
Mixing can start as purely homogeneous	Any mixing starts with the inhomogeneous stage
Homogeneous mixing leads to a DSD shift to small droplet sizes	Homogeneous mixing does not always lead to the DSD shift to small droplet sizes (Pt. 2). The shift depends on the DSD shape.
Mixing can be analyzed within the framework of a monodisperse DSD	Mixing always leads to formation of polydisperse DSD
In the course of homogeneous mixing, droplet concentration remains constant	In the course of homogeneous mixing, droplet concentration does not always remain constant (Pt. 2)
Extremely inhomogeneous mixing does not change the DSD shape	Inhomogeneous mixing (including extremely inhomogeneous) leads to broadening of the DSD towards small sizes

<p>In the course of inhomogeneous mixing, the effective radius remains constant</p>	<p>The effective radius varies only slightly (5-20 %) in the initially cloud volume. The effective radius rapidly increases in the initially droplet-free volume, approaching the value of effective radius in the cloud volume. With increasing <math>Da</math>, the difference between the values of the effective radius in the initially cloud volume and that at the final state decreases in agreement with the classic concept.</p>
---	--

1316

1317

1318

1319

1320

1321

1322

1323

1324

1325

1326

1327

1328

1329

1330

1331

1332

1333

**Tab. A. List of symbols**

1334

("nd" means non-dimensional)

Symbol	Description	Units
$A_2$	$\frac{1}{q_v} + \frac{L_w^2}{c_p R_v T^2}$ , coefficient	nd
$a_0, a_n$	the Fourier series coefficients	nd
$C$	the Richardson's law constant	nd
$c_p$	specific heat capacity of moist air at constant pressure	$\text{J kg}^{-1} \text{K}^{-1}$
$\mathcal{D}$	coefficient of water vapour diffusion in the air	$\text{m}^2 \text{s}^{-1}$
$Da$	the <i>Damköhler</i> number	nd
$e$	water vapor pressure	$\text{N m}^{-2}$
$e_s$	saturation vapour pressure above a flat water surface	$\text{N m}^{-2}$
$F$	$F = \frac{\rho_w L_w^2}{k_a R_v T^2} + \frac{\rho_w R_v T}{e_s(T) \mathcal{D}}$ , coefficient	$\text{m}^{-2} \text{s}$
$f(r)$	droplet size distribution	$\text{m}^{-4}$
$g(\sigma)$	distribution of square radius	$\text{m}^{-5}$
$\tilde{g}(\tilde{\sigma})$	normalized distribution of square radius	nd
$k_a$	coefficient of air heat conductivity	$\text{J m}^{-1} \text{s}^{-1} \text{K}^{-1}$
$K$	turbulent diffusion coefficient	$\text{m}^2 \text{s}^{-1}$
$L$	characteristic spatial scale of mixing	m
$L_w$	latent heat for liquid water	$\text{J kg}^{-1}$
$m_\alpha$	moment of DSD of order $\alpha$	$\text{m}^{-3}$
$N$	droplet concentration	
$\tilde{N}$	normalized droplet concentration	nd
$N_1$	Initial droplet concentration in a cloud volume	$\text{m}^{-3}$
$p$	pressure of moist air	$\text{N m}^{-2}$
$q$	liquid water mixing ratio	kg/kg
$q_1$	Initial liquid water mixing ratio in a cloudy volume	kg/kg
$q_v$	water vapor mixing ratio	kg/kg
$\tilde{q}$	normalised liquid water mixing ratio equal to	nd



	normalized LWC	
$r$	droplet radius	m
$r_0$	initial droplet radius	m
$r_0$	mean droplet radius	m
$r_v$	mean volume radius	m
$R$	$\frac{S_2}{A_2 q_1}$ , potential evaporation parameter (PEP)	nd
$R_a$	specific gas constant of moist air	$\text{J kg}^{-1} \text{K}^{-1}$
$R_v$	specific gas constant of water vapor	$\text{J kg}^{-1} \text{K}^{-1}$
$S$	$e/e_w - 1$ , supersaturation over water	nd
$\tilde{S}$	normalized supersaturation	nd
$S_2$	Initial supersaturation in a dry volume	nd
$\tilde{S}_{\max}$	maximal normalized supersaturation	nd
$T$	temperature	K
$T_{\text{mix}}$	normalized duration of inhomogeneous stage	nd
$T_{\text{ev}}$	normalized duration of evaporation	nd
$T_{\text{tot}}$	normalized duration of mixing	nd
$t$	time	s
$\tilde{t}$	non-dimensional time	nd
$x$	distance	m
$\tilde{x}$	non-dimensional distance	nd
$\lambda_1, \lambda_2$	criteria of delimitation between the types of mixing	nd
$\varepsilon$	turbulent dissipation rate	$\text{m}^2 \text{s}^{-3}$
$\Gamma(x, t)$	conservative function	nd
$\tilde{\Gamma}$	normalized conservative function	nd
$\rho_a$	air density	$\text{kg m}^{-3}$
$\rho_w$	density of liquid water	$\text{kg m}^{-3}$
$\sigma$	square of droplet radius	$\text{m}^2$
$\tilde{\sigma}$	normalized square of droplet radius	nd
$\tau_{pr}$	phase relaxation time	s

$\tilde{\tau}_{pr}$	normalized phase relaxation time	nd
$\tau_{mix}$	characteristic time of mixing	s
$\tau_0$	Initial time scale	s

1335

1336

1337

1338

1339

1340

1341

1342

1343

1344

1345

1346

1347

1348

1349

1350

1351

1352

1353

1354

1355

1356

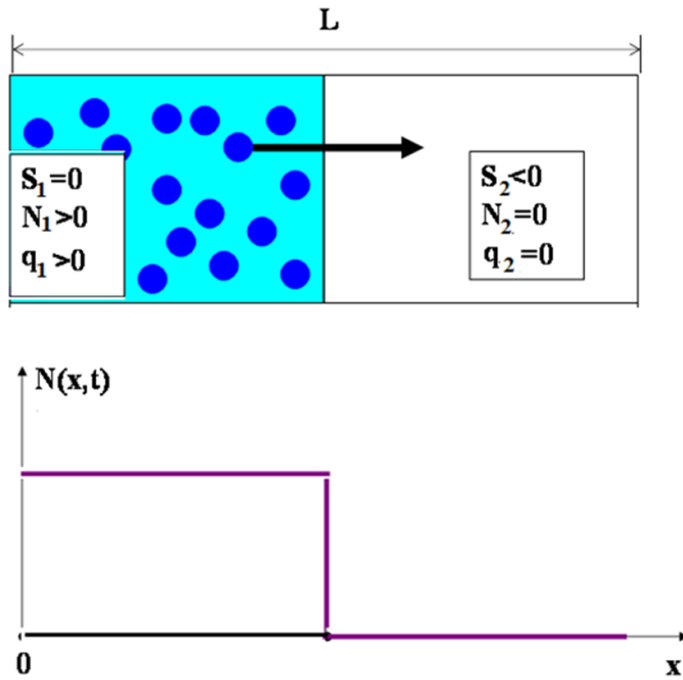
1357

1358 **Figures**

1359

1360

1361



1362

1363

1364 **Fig.1.** The schematic illustration of the 1D mixing problem considered in the study. The  
 1365 initial state at  $t = 0$  is illustrated. The left volume of length  $L/2$  is a saturated cloudy volume;  
 1366 the right volume is a non-saturated air volume from the cloud environment.

1367

1368

1369

1370

1371

1372

1373

1374

1375

1376

1377

1378

1379

1380

1381

1382

1383

1384

1385

1386

1387

1388

1389

1390

1391

1392

1393

1394

1395

1396

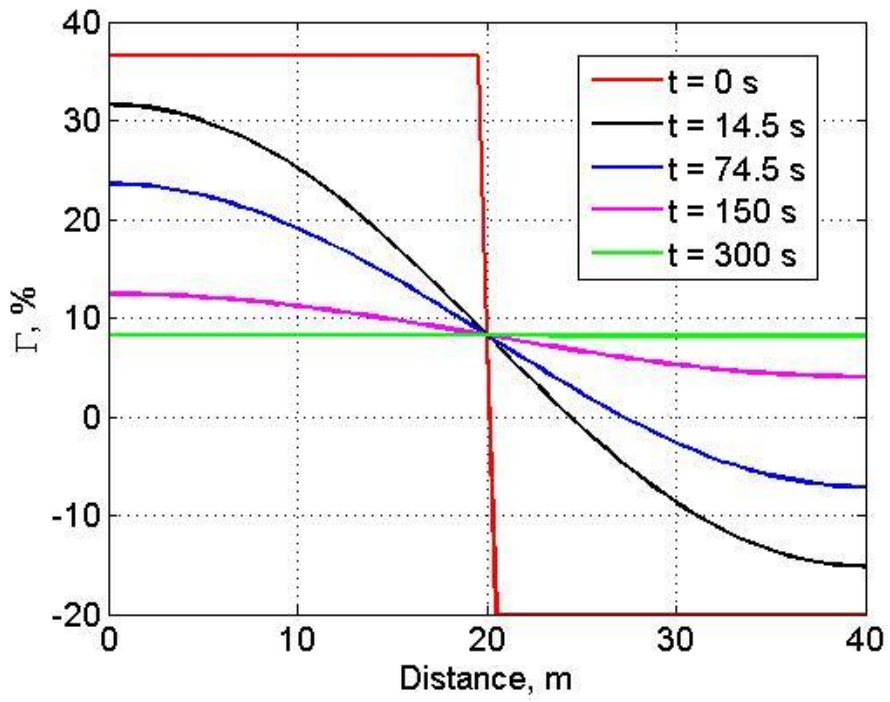


**Fig. 2.** An example of  $\Gamma(x,t)$  evolution during mixing.

1397

1398

1399

1400

1401

1402

1403

1404

1405

1406

1407

1408

1409

1410

1411

1412

1413

1414

1415

1416

1417

1418

1419

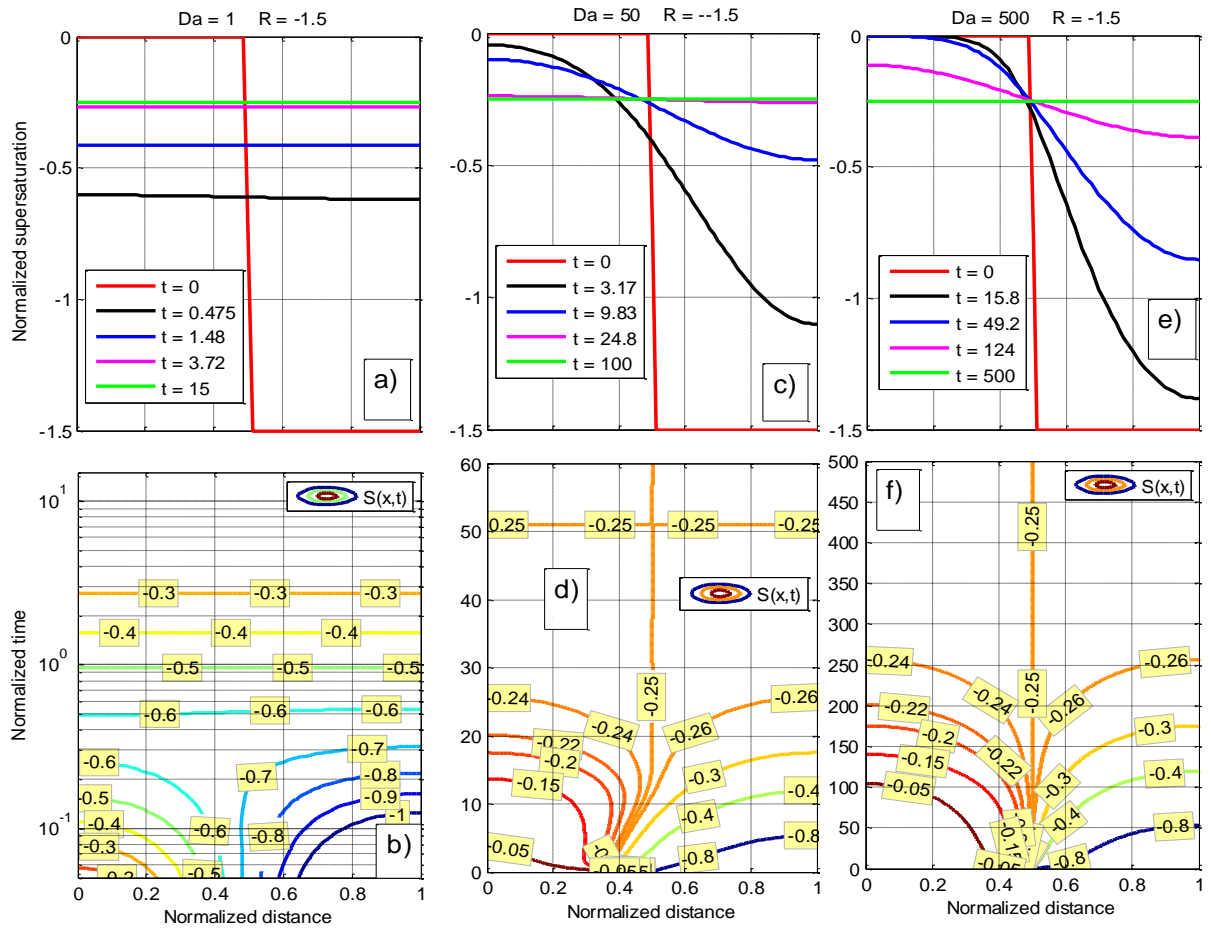
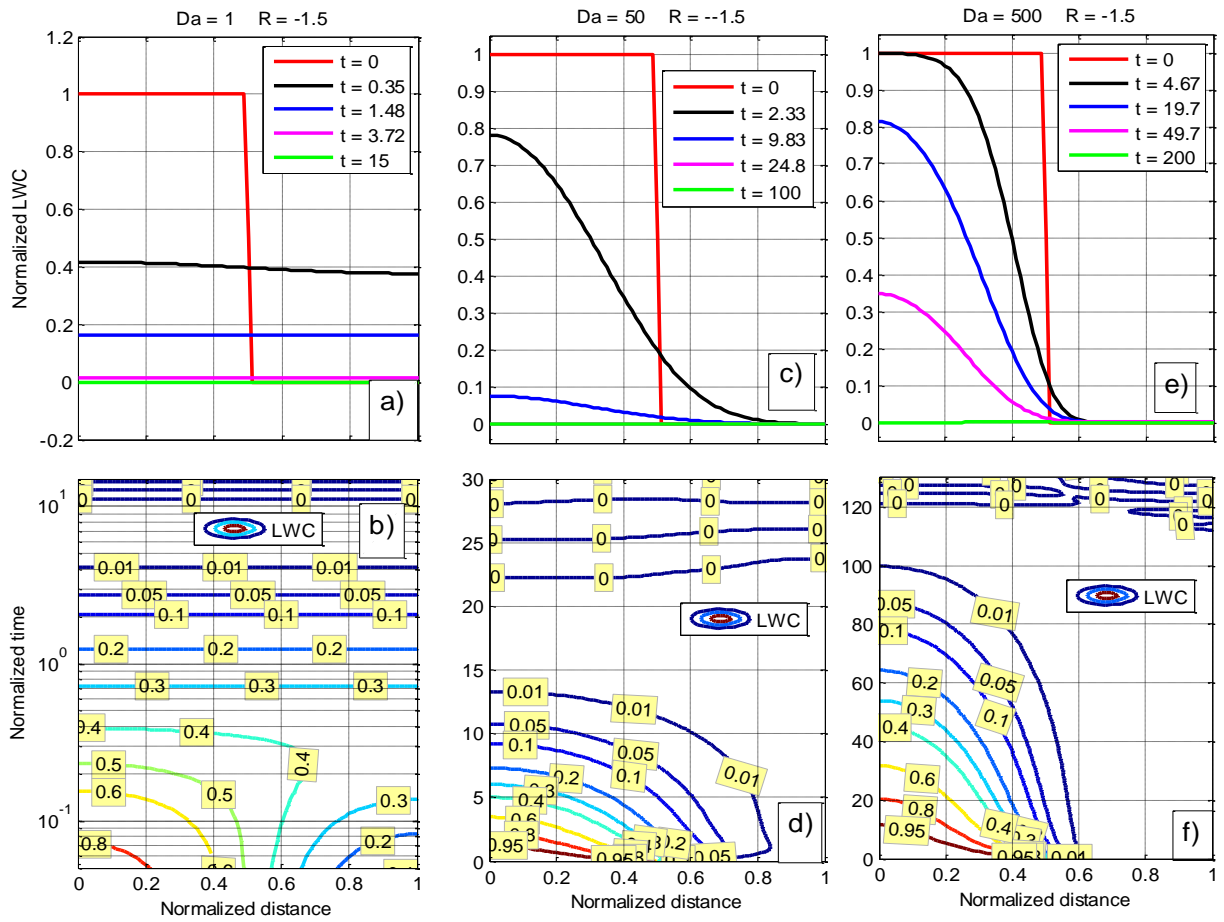


**Fig. 3.** Horizontal dependencies (upper row) and  $\tilde{x}-\tilde{t}$  dependencies (lower row) of normalized supersaturation at  $Da = 1$ ,  $Da = 50$  and  $Da = 500$  and at  $R = -1.5$ . Panel b is plotted in semi-log scale.

1420



1421

1422

1423

1424

1425 **Fig. 4.** The same as in Fig. 3, but for normalized LWC. Left bottom panel is plotted in

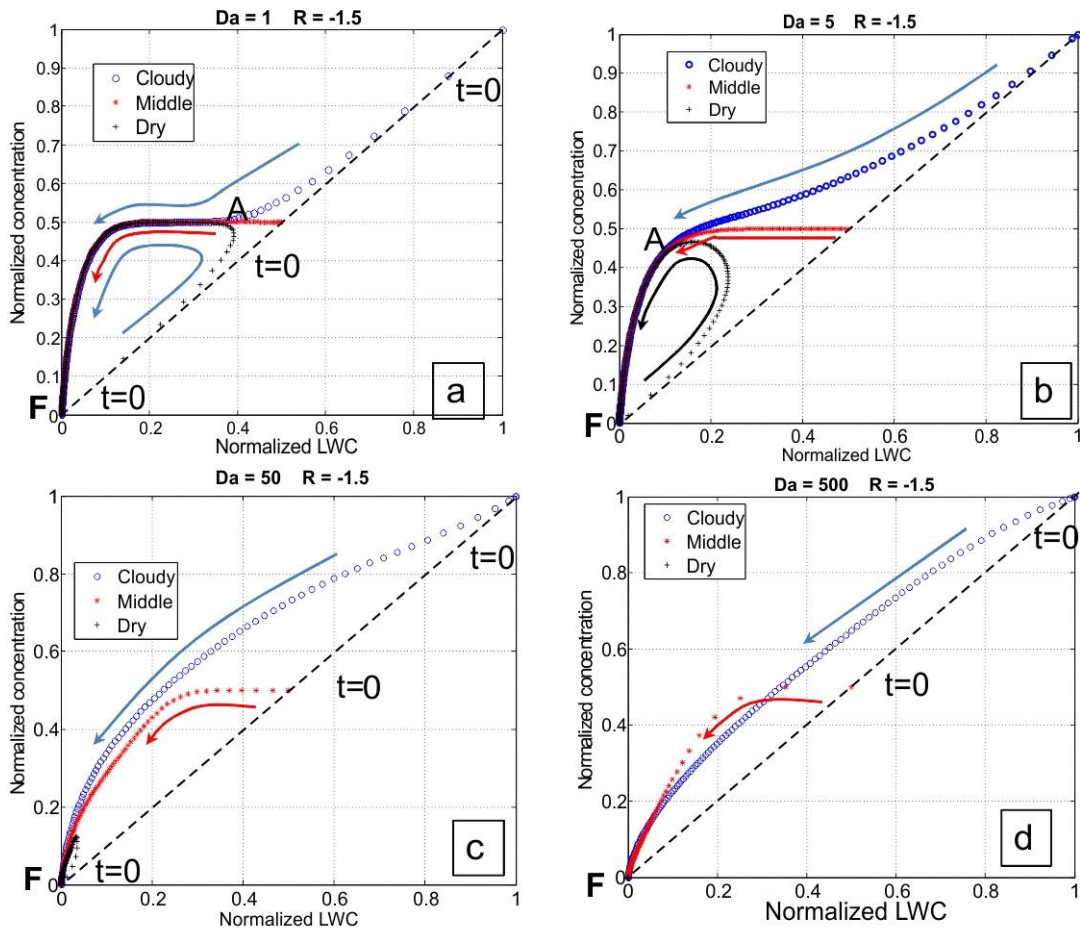
1426 semi-log scale.

1427

1428

1429

1430



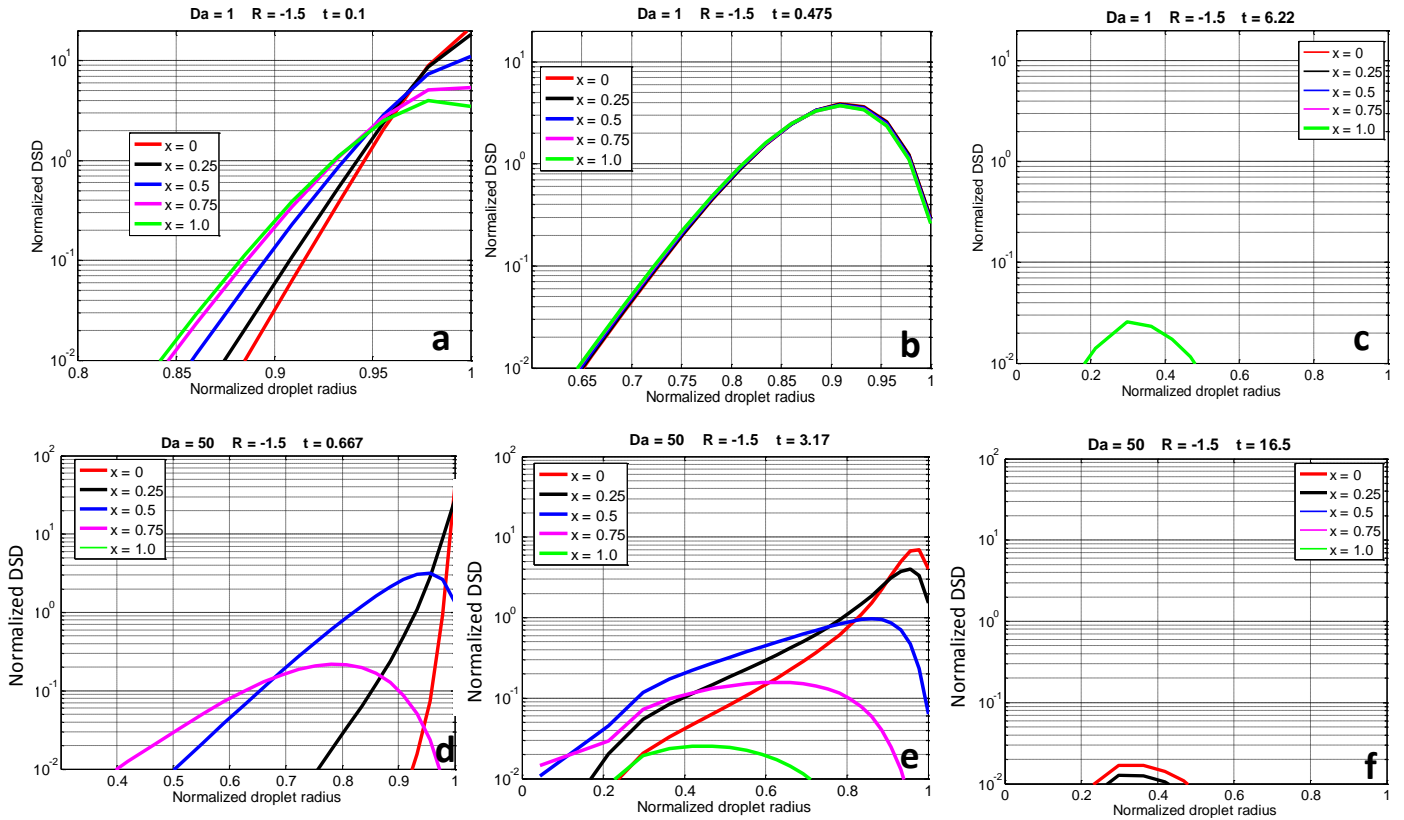
1431

1432 **Fig. 5.** Dependencies of normalized values of droplet concentration on normalized LWC  
 1433 at different  $Da$  and  $R = -1.5$ . Blue symbols mark the centre of the cloudy volume ( $\tilde{x} = 1/4$ ),  
 1434 red symbols mark the interface between the cloudy volume and the dry volume ( $\tilde{x} = 1/2$ ), and  
 1435 black crosses mark the centre of the initially droplet-free volume ( $\tilde{x} = 3/4$ ). Symbols are  
 1436 plotted at different time instances. Symbols at  $t=0$  show initial values of droplet concentration  
 1437 and LWC at the three values of  $\tilde{x}$ . Arrows show the direction of movement of the points at the  
 1438 diagram with time. Point "A" marks the beginning of the spatially homogeneous stage,  $\tilde{t} = T_{mix}$ .  
 1439 Point "F" marks the final state. The dashed line indicates the relationship between  $\tilde{N}$  and  $\tilde{q}$  in  
 1440 extremely inhomogeneous mixing (according to the classical concept).

1441

1442

1443



1444

1445

1446 **Fig. 6** Time evolution of DSD during droplet evaporation at  $Da=1$  (upper row) and  
 1447  $Da=50$  (bottom row). In each panel, the normalized DSD are shown at different values of  
 1448 horizontal coordinate  $\tilde{x}$ . Different panels show DSD at different time instances.

1449

1450

1451

1452

1453



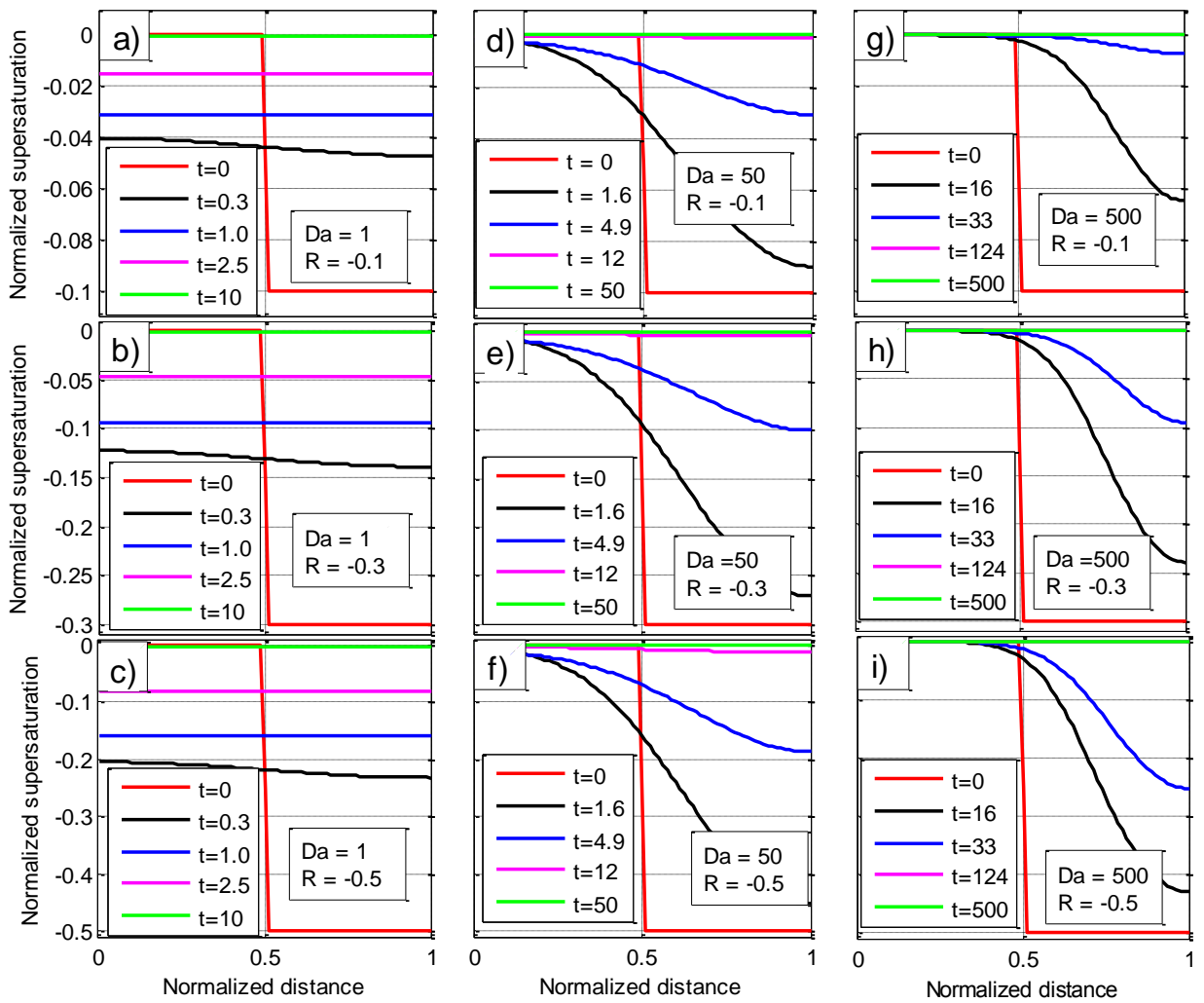


**Fig. 7.** Profiles of normalized supersaturation at different  $Da$  and different  $R > -1$ .

1475

1476

1477

1478

1479

1480

1481

1482

1483

1484

1485

1486

1487

1488

1489

1490

1491

1492

1493

1494

1495

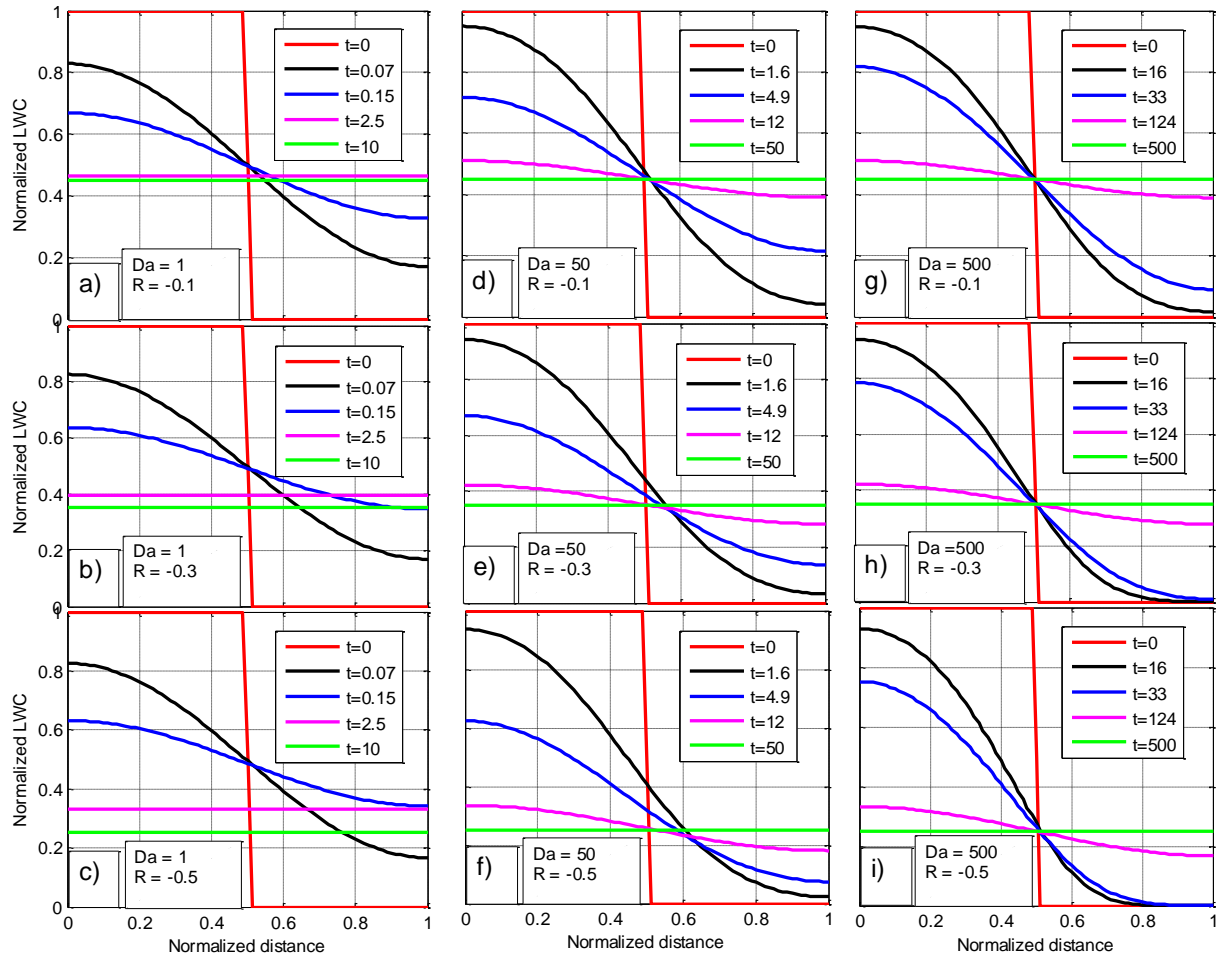


**Fig. 8.** Profiles of normalized LWC at different  $Da$  and at different  $R > -1$ .

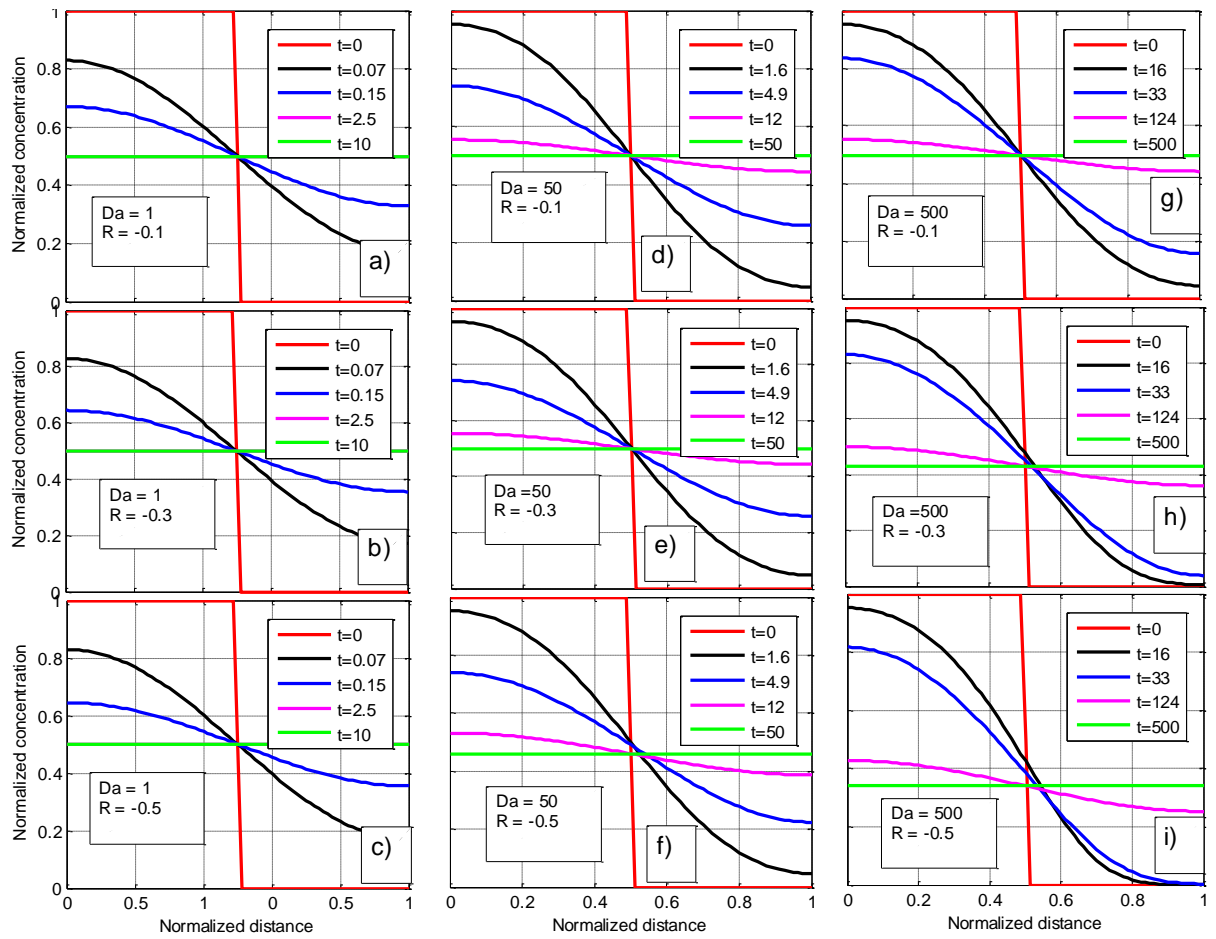
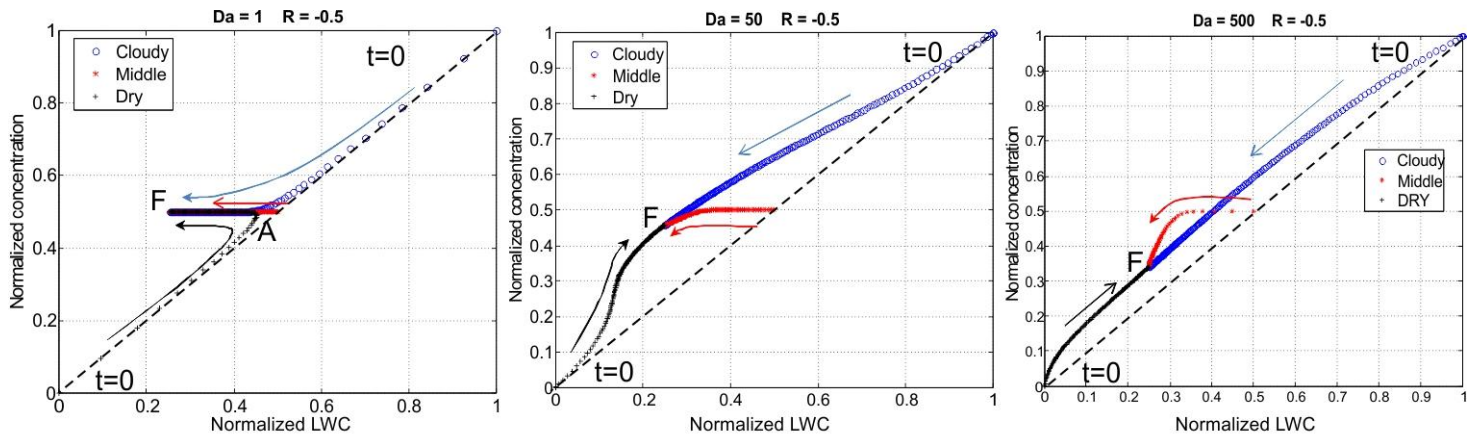


**Fig. 9.** Profiles of normalized droplet concentration at different  $Da$  and at different  $R > -1$ .

1521

1522

1523



1524

1525

1526 **Fig. 10.** Dependencies of normalized values of droplet concentration on normalized LWC  
 1527 at different  $Da$  and at  $R = -0.5$ . Blue circles mark the centre of the cloudy volume ( $\tilde{x} = 1/4$ ),  
 1528 red symbols mark the initial interface ( $\tilde{x} = 1/2$ ) and black crosses mark the centre of the  
 1529 initially dry volume ( $\tilde{x} = 3/4$ ). Arrows show the direction of movement of the points with  
 1530 time. Point “F” marks the final stationary state of the system. The dashed line indicates the  
 1531 relationship between  $\tilde{N}$  and  $\tilde{q}$  in extremely inhomogeneous mixing (according to the classical  
 1532 concept).

1533

1534

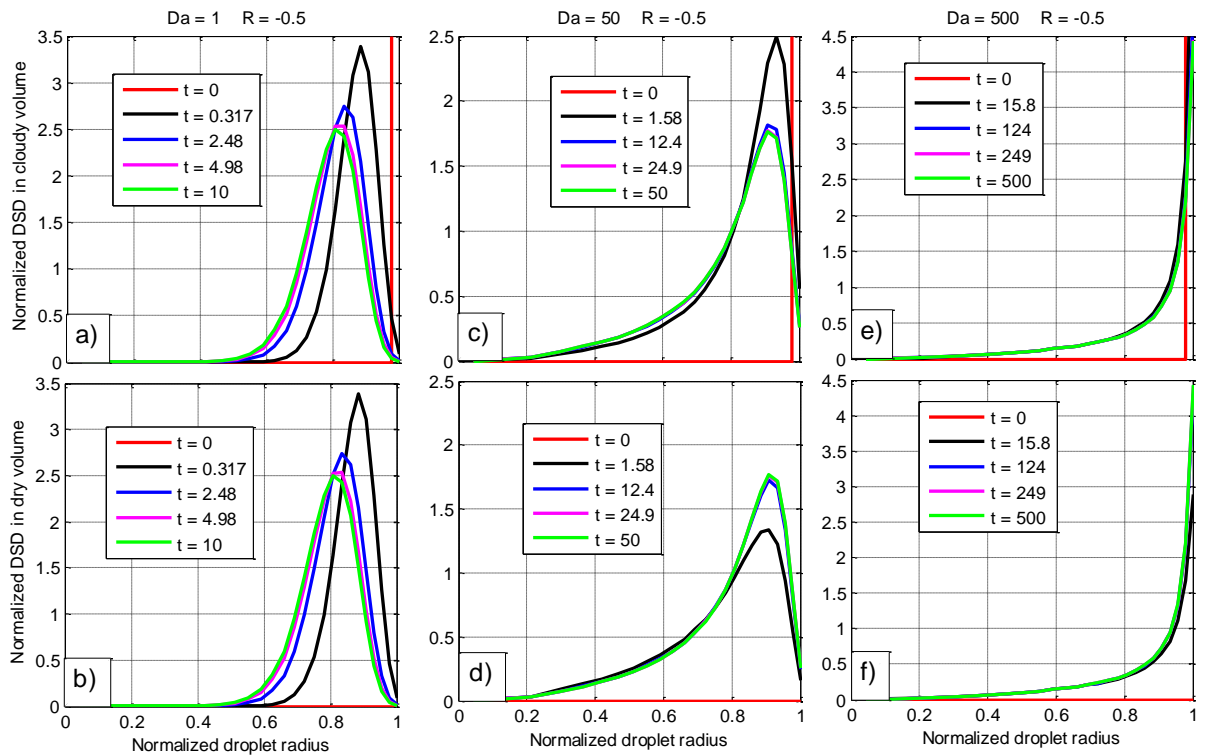
1535

1536

1537

1538

1539



1540

1541

1542 **Fig. 11** Examples of DSD evolution in the initially cloudy volume ( $\tilde{x} = 1/4$ ) (upper row)1543 and in the initially dry volume ( $\tilde{x} = 3/4$ ) (lower row) at  $R = -0.5$  and at different values of1544  $Da$ .

1545

1546

1547

1548

1549

1550

1551

1552

1553

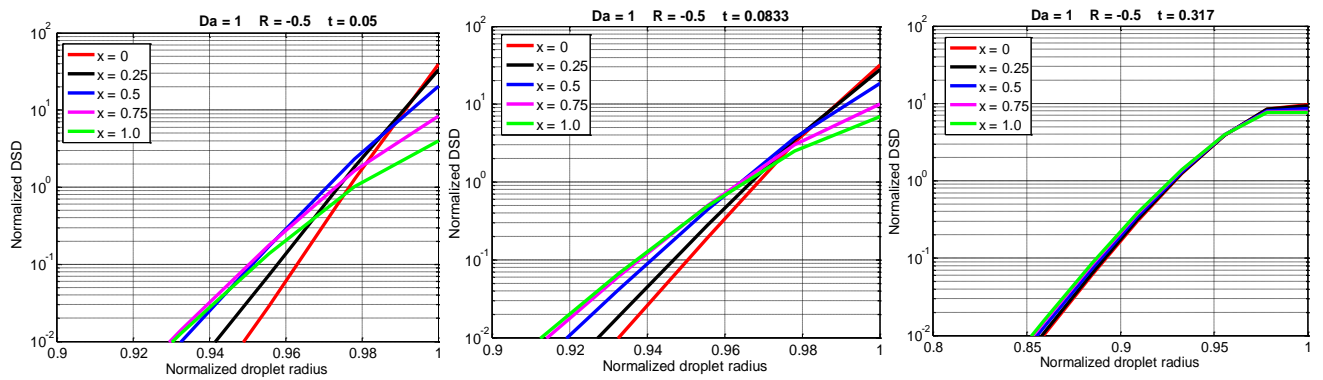
1554

1555

1556

1557

1558



1559

1560

1561

1562

1563

1564

1565

1566

1567

1568

1569

1570

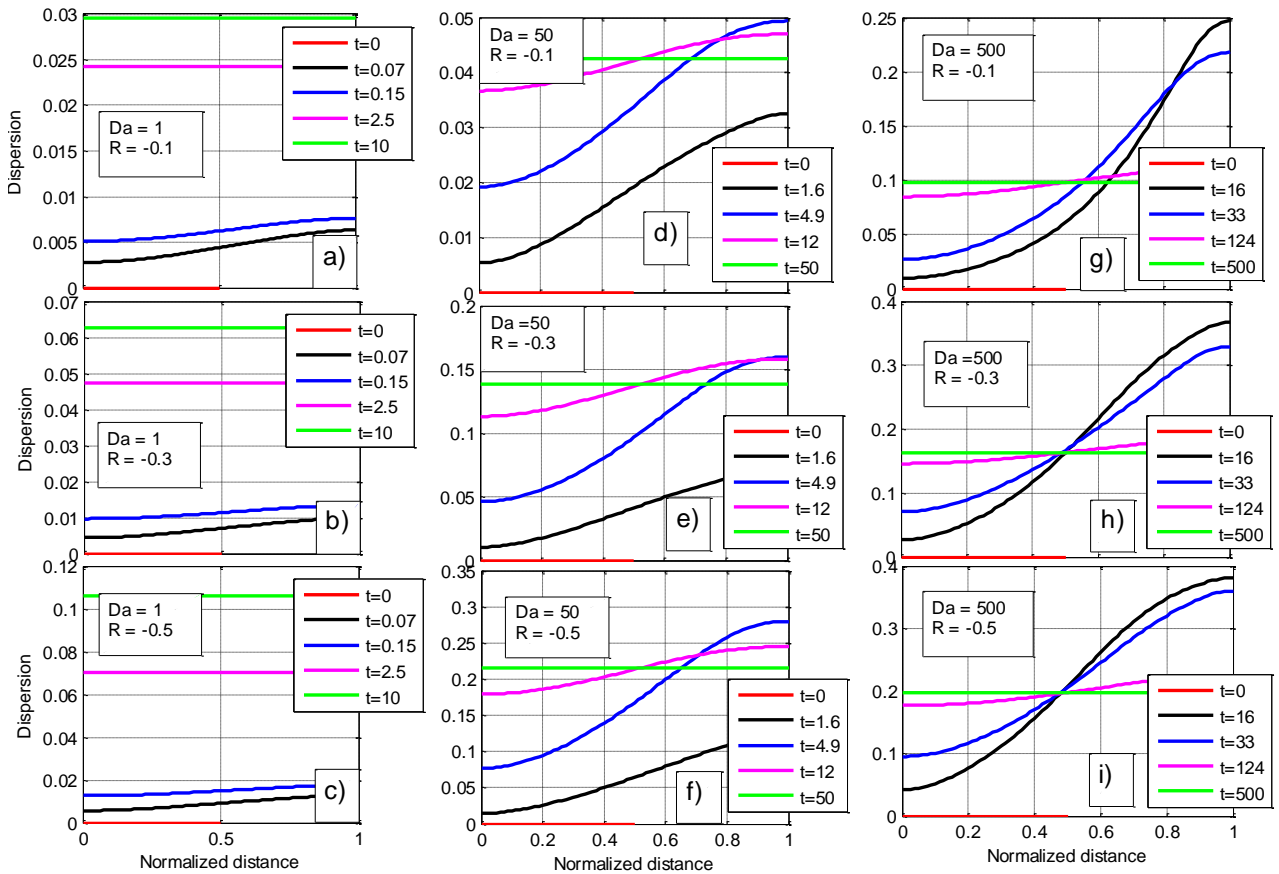
**Fig. 12.** DSD at different  $\tilde{x}$  at the beginning of the mixing process for  $Da=1$  and  $R=-0.5$ .

1571

1572

1573

1574



1575

1576

1577 **Fig. 13.** Spatial dependencies of the relative DSD dispersion at different time instances and

1578 at different values of  $Da$  and different  $R > -1$

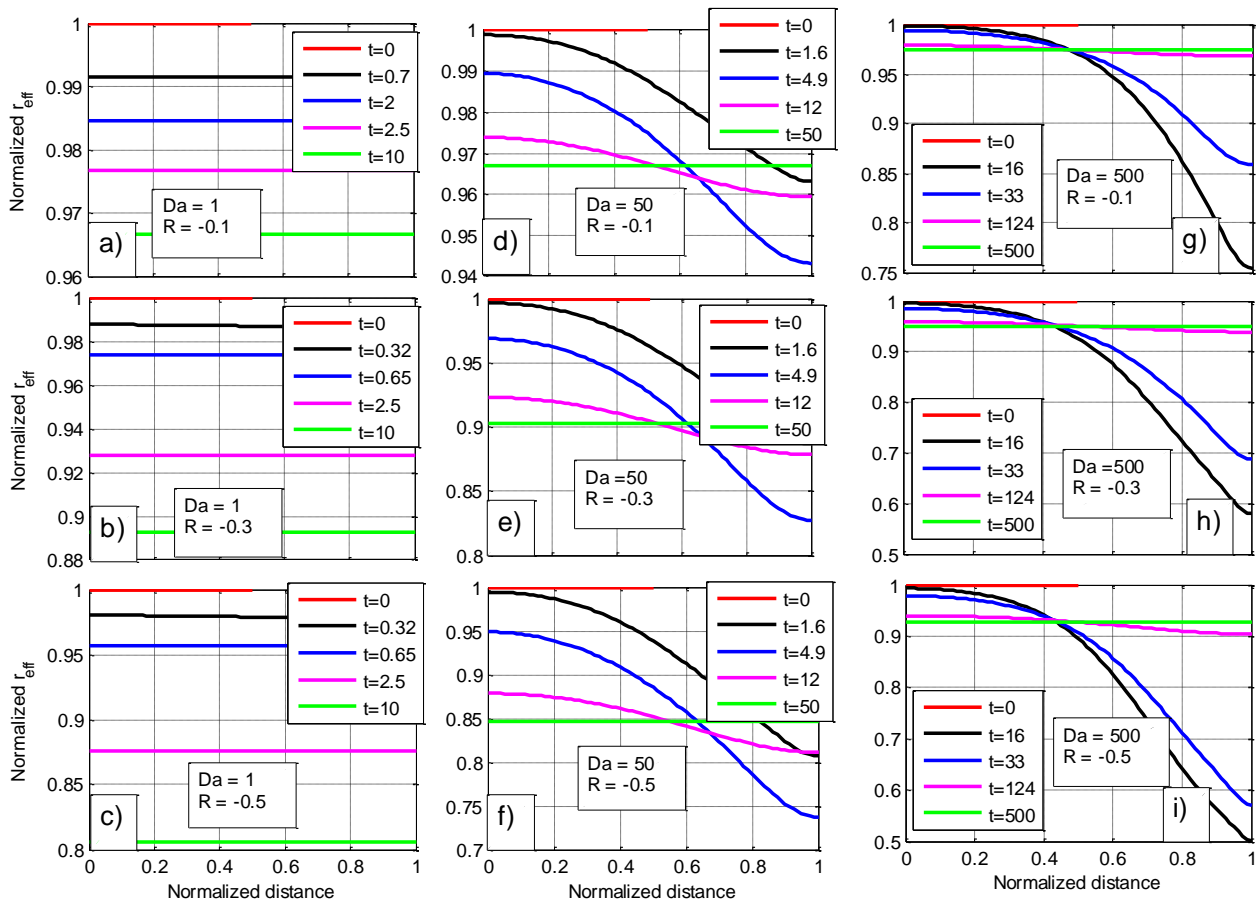
1579

1580

1581

1582

1583



1584

1585

1586 **Fig. 14.** Spatial dependencies of the effective radius at different time instances and at  
 1587 different values of  $Da$  and different  $R > -1$

1588

1589

1590

1591

1592

1593

1594



1595

1596

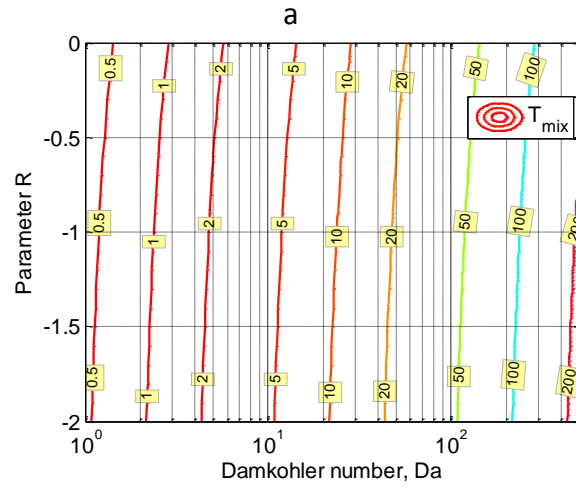
1597

1598

1599

1600

1601



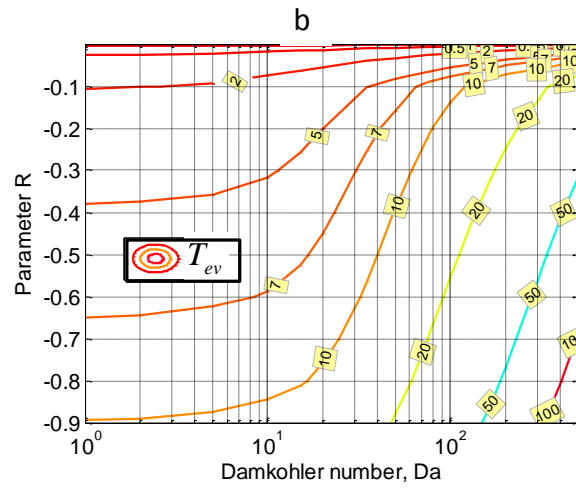
1602

1603

1604

1605

1606



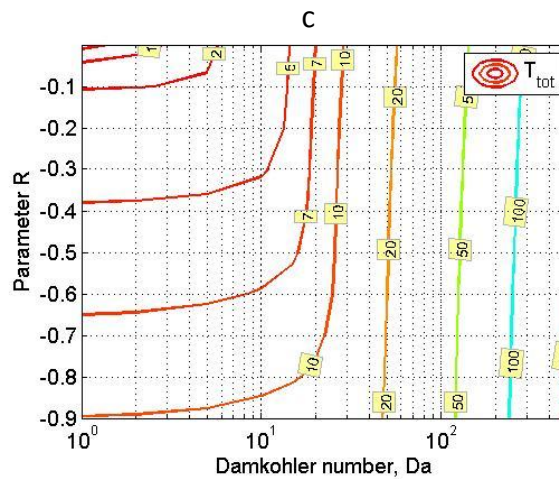
1607

1608

1609

1610

1611



1612

1613 **Fig. 15.** Contours of normalized mixing duration times on  $Da-R$  plane. (a) mixing time

1614  $T_{mix}$ , (b) evaporation time  $T_{ev}$ , and (c) the total duration mixing time  $T_{tot}$ .

1615

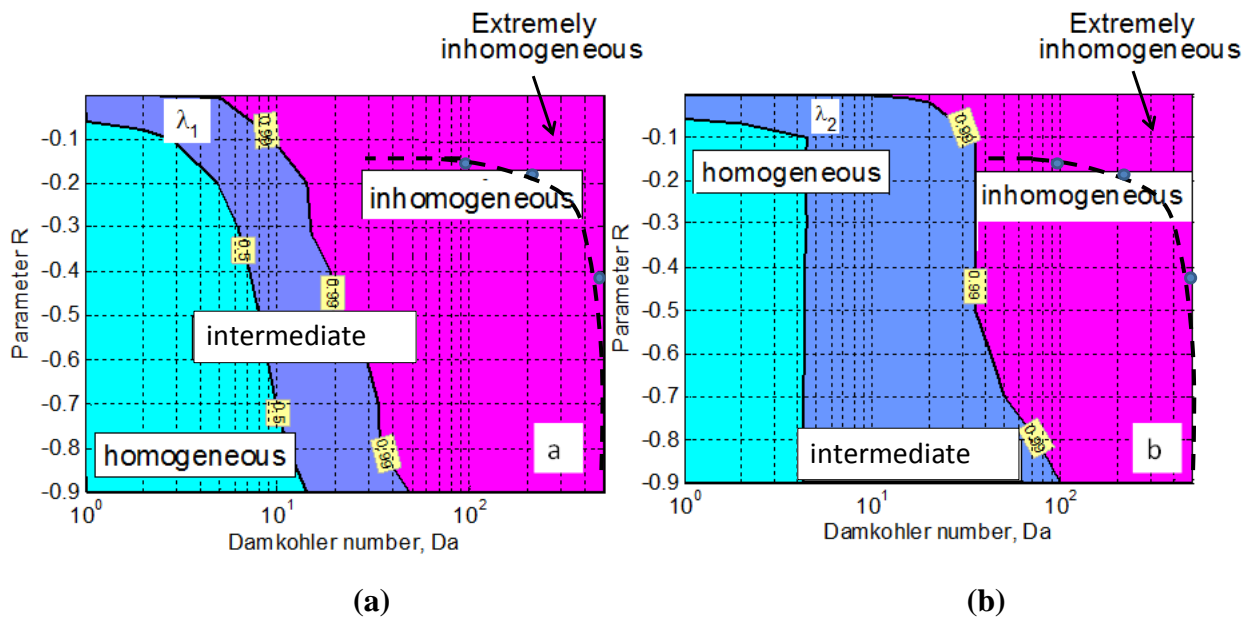


**Fig. 16.** (a) The boundaries between mixing types on the  $Da - R$  plane designed according to criteria  $\lambda_1 = \frac{T_{mix}}{T_{tot}}$ ; (b) The boundaries between mixing types on the  $Da - R$  plane designed according to criterion  $\lambda_2 = \frac{2\langle\tilde{q}(T_{mix})\rangle - 1}{R}$  (Eq. 41). Dashed lines indicate the line corresponding to 2% deviation from the initial mean volume radius.

1639

1640

1641

1642

1643

1644

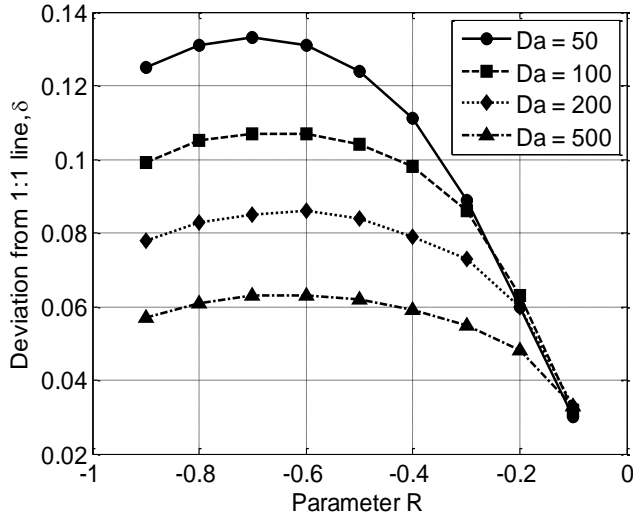
1645

1646

1647

1648

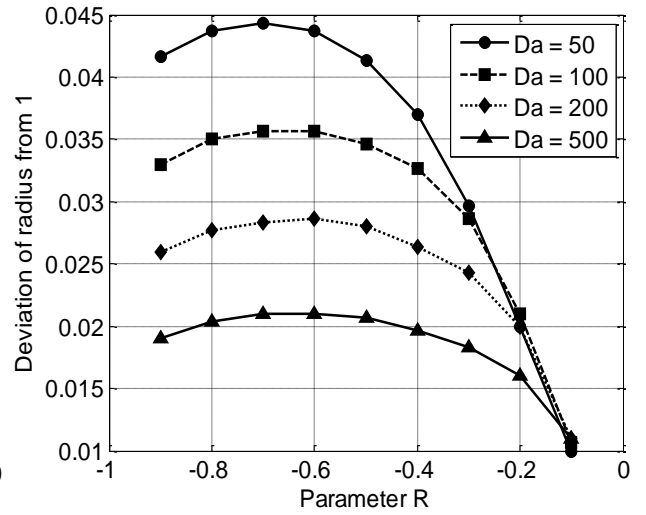
1649



1650

1651

(a)



1652

1653

1654

1655

1656

1657

1658

(b)

**Fig 17.** (a) Dependencies of the r.m.s. distance of the  $\tilde{N} - \tilde{q}$  relationship curve from straight line 1:1 suggested by classical concept of extremely inhomogeneous mixing. The dependencies are plotted for different values of  $Da$  and  $R$ . (b) The same as to the left panel but for r.m.s. deviations of the mean volume radius curve from that initial constant value assumed in the classical concept.